

1 **A potent alpaca-derived nanobody that neutralizes SARS-CoV-2 variants**

2 Jules B. Weinstein<sup>1,\*</sup>, Timothy A. Bates<sup>1,\*</sup>, Hans C. Leier<sup>1</sup>, Savannah K. McBride<sup>1</sup>, Eric Barklis<sup>1</sup>,

3 Fikadu G. Tafesse<sup>1,#</sup>

4

5 <sup>1</sup>Department of Molecular Microbiology and Immunology, Oregon Health and Sciences

6 University, 3181 SW Sam Jackson Park Road, Portland, OR, 97239-3098, USA.

7

8 \*These authors contributed equally to this publication

9 #Corresponding author: Fikadu G. Tafesse ([tafesse@ohsu.edu](mailto:tafesse@ohsu.edu))

10

11 **Abstract**

12 The spike glycoprotein of SARS-CoV-2 engages with human angiotensin-converting enzyme 2  
13 (ACE2) to facilitate infection. Here, we describe an alpaca-derived heavy chain antibody  
14 fragment (VHH), saRBD-1, that disrupts this interaction by competitively binding to the spike  
15 protein receptor-binding domain. We further generated an engineered bivalent nanobody  
16 construct engineered by a flexible linker, and a dimeric Fc conjugated nanobody construct. Both  
17 multivalent nanobodies blocked infection at picomolar concentrations and demonstrated no loss  
18 of potency against emerging variants of concern including Alpha (B.1.1.7), Beta (B.1.351),  
19 Gamma (P.1), Epsilon (B.1.427/429), and Delta (B.1.617.2). saRBD-1 tolerates elevated  
20 temperature, freeze-drying, and nebulization, making it an excellent candidate for further  
21 development into a therapeutic approach for COVID-19.

22

## 23 **Introduction**

24 The COVID-19 pandemic, caused by severe acute respiratory syndrome coronavirus-2 (SARS-  
25 CoV-2), is an ongoing global health crisis with over 230 million cases, 4.8 million deaths world-  
26 wide as of October 2021 (Dong et al., 2020). While several effective vaccines have been  
27 developed, concern about potential future surges of infections remain, due to the proliferation  
28 and spread of multiple variant strains, combined with waning protection from vaccination (Levin  
29 et al., 2021; Shrotri et al., 2021). It is anticipated that additional variants will continue to emerge,  
30 and the slow pace of global vaccination creates greater opportunity for emergence and spread  
31 of vaccine resistant variants (Luo et al., 2021).

32

33 SARS-CoV-2 is an enveloped, positive-sense, single-stranded RNA virus, and a member of the  
34 Coronaviridae family, so named for the crown-like protrusions visible on their outer membranes  
35 in EM micrographs (Huang et al., 2020). Four structural proteins are encoded by SARS-CoV-2:  
36 spike (S), envelope, membrane, and nucleocapsid (Jiang et al., 2020). Homotrimers of the S  
37 glycoprotein form the characteristic crown-like protrusions on the virion surface, where it  
38 facilitates entry into cells through its interaction with the cell surface protein angiotensin-  
39 converting enzyme 2 (ACE2) (Hoffmann et al., 2020). Each monomer of S is composed of two  
40 subunits, S1 and S2, the former being responsible for ACE2 binding, and the latter involved in  
41 membrane fusion with target cells. These subunits are connected by a polybasic cleavage site,  
42 which is typically cleaved by the human cell surface-bound protease, TMPRSS2, releasing the  
43 S1 subunit to reveal the fusion peptide of S2 (Hoffmann et al., 2020). Many neutralizing  
44 antibodies function by binding to the receptor binding domain (RBD) of the S1 subunit, thereby  
45 blocking ACE2 engagement and preventing protease activation of fusion-competent S2 (Carrillo  
46 et al., 2021).

47

48 Neutralizing antibodies have been shown to be protective against COVID-19 disease (Khoury et  
49 al., 2021), and a majority of the treatment options approved for emergency use by the United  
50 States Food and Drug Administration for severe COVID-19 consist of monoclonal antibody  
51 cocktails (Kumar et al., 2021). The advantage of monoclonal antibodies is their ability to prevent  
52 entry of the virus into cells through their highly specific interaction with the spike protein (Jiang  
53 et al., 2020). This effectively limits the ability of SARS-CoV-2 to infect cells with minimal risk of  
54 side effects (Weinreich et al., 2021). The disadvantages of monoclonal antibody treatments are  
55 the difficulties of their production, high cost, and the possibility of escape by variants.

56 Several SARS-CoV-2 variants have displayed a propensity for increased transmission, as well  
57 as evasion of antibody neutralization by immune sera. The most clinically important of these are  
58 the variants of concern (VOC) including Alpha (B.1.1.7) (Bates et al., 2021a; Liu et al., 2021a;  
59 Planas et al., 2021), Beta (B.1.351) (Bates et al., 2021a), Gamma (P.1) (Bates et al., 2021b;  
60 Hoffmann et al., 2021), Delta (B.1.617.2) (Liu et al., 2021b), Epsilon (B.1.427/429) (Deng et al.,  
61 2021) and Omicron (B.1.529) (Liu et al., 2021c; Zhang et al., 2021); each of which has  
62 demonstrated significant immune evasion. These variants all incorporate numerous amino acid  
63 substitutions that are responsible for altering the epitopes critical for antibody-based  
64 neutralization. Previous work has shown that antibody cross-reactivity is common between  
65 different coronaviruses (Yuan et al., 2020). However, cross-neutralization is rare, and while  
66 some cross-neutralizing antibodies have been described (Pinto et al., 2020), even strongly  
67 binding cross-reactive antibodies are not necessarily neutralizing (Bates et al., 2021c).

68

69 One promising new technology that overcomes some of the inherent disadvantages of  
70 traditional monoclonal antibodies are nanobodies, which are immune fragments derived from  
71 the unique heavy-chain-only antibodies found in camelid species such as alpacas (Ingram et al.,  
72 2018). Composed solely of the heavy-chain only antibody variable domains (VHH), nanobodies  
73 are one-tenth the size of conventional antibodies, while preserving their binding affinities

74 (Ingram et al., 2018). As single peptides with no need for glycosylation or complex maturation  
75 pathways, nanobodies offer several key advantages such as higher throughput discovery,  
76 simplified production, and improved stability. Because they lack antibody constant domains,  
77 nanobodies also avoid Fc-mediated immune activation (Salvador et al., 2019).

78

79 In this report, we detail the development of an alpaca-derived anti-SARS-CoV-2 nanobody  
80 (saRBD-1) with picomolar binding to the RBD portion of the spike protein. saRBD-1 displays  
81 high thermostability and remains functional after nebulization. Unmodified monovalent saRBD-1,  
82 bivalent saRBD-1, and a bivalent IgG Fc conjugated saRBD-1 protein all successfully neutralize  
83 live SARS-CoV-2 clinical isolates including the VOCs Alpha, Beta, Gamma, Epsilon, and Delta  
84 with no loss of potency. Variant cross-reactive nanobodies such as saRBD-1 may have  
85 therapeutic potential in COVID-19 caused by SARS-CoV-2 variants.

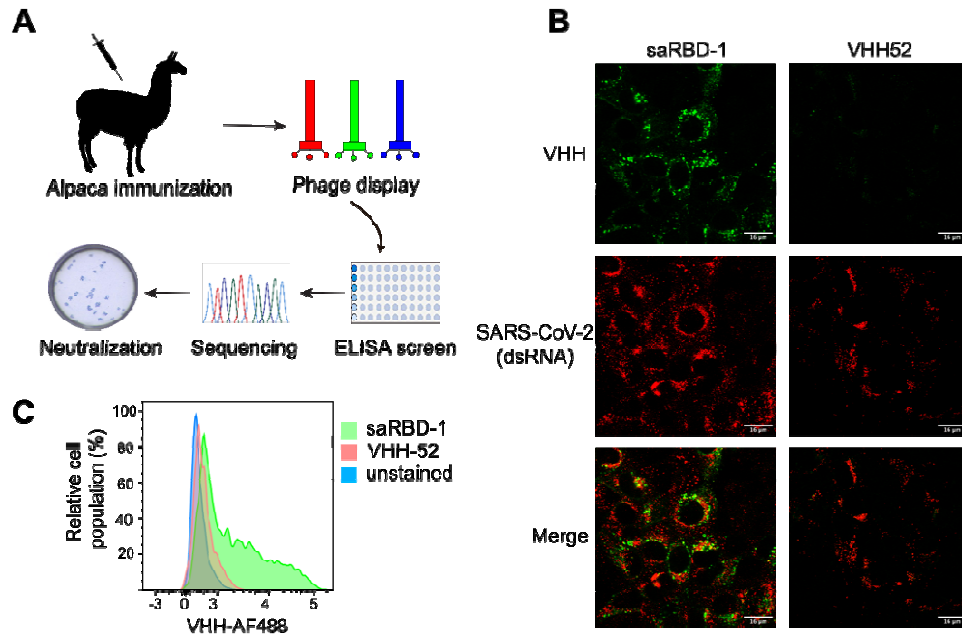
86

## 87 **Results**

### 88 **A dominant VHH clone that binds SARS-COV-2 spike, saRBD-1 was isolated from spike** 89 **RBD immunized alpaca**

90 To acquire potent SARS-CoV-2 neutralizing VHHs, we first immunized an alpaca with purified  
91 SARS-CoV-2 S RBD. We used standard immunization techniques (Maass et al., 2007) over a  
92 50-day immunization schedule, after which we generated a VHH gene library from immunized  
93 alpaca peripheral blood mononuclear cells (PBMCs), from which we isolated S binding VHH  
94 genes via phage display (Figure 1A). We performed panning against purified full-length trimeric  
95 S protein to maximize the number of native epitopes that match those present on live SARS-  
96 CoV-2 virus. Two rounds of panning enriched high binders in our library population. High quality  
97 hits were identified by high-throughput enzyme-linked immunosorbent assays (ELISA) of  
98 individual VHH clones on immobilized RBD. VHH hits which showed binding significantly above  
99 background were sequenced to determine their unique complementary-determining region 3

100 (CDR3) loops. Resulting high binding VHH sequence families with an enrichment of 10% or  
101 more after panning were tested for neutralizing activities. Neutralization assays used a GFP-  
102 reporter lentivirus pseudotyped with SARS-CoV-2 S protein (Crawford et al., 2020). Human  
103 ACE2 over-expressing HEK-293T cells (293T-ACE2) were incubated with pseudotyped virus in  
104 the presence of candidate VHHS. From our initial candidate pool, we discovered one novel VHH  
105 clone, referred to here as saRBD-1, that completely neutralized spike-mediated lentivirus  
106 transduction (Figure S1). We next analyzed the ability of saRBD-1 to associate with SARS-CoV-  
107 2 S using flow cytometry and immunofluorescence. African green monkey kidney cells (Vero  
108 E6) cells were infected with live SARS-CoV-2 WA1/2020 strain, then stained with anti-dsRNA  
109 monoclonal antibody to identify infected cells, and saRBD-1 or a control VHH (VHH52)  
110 (Cavallari, 2017) (Figure 1B). Cells positive for SARS-CoV-2 dsRNA showed concomitant  
111 binding by saRBD-1, but not VHH52 control. In a thermal shift assay, we found that equimolar  
112 saRBD-1 stabilized RBD protein and shifted the melting point by 8°C, from 52°C to 60°C (Figure  
113 S2). From this assay, we also determined that the melting point of saRBD-1 is 72°C in plain  
114 phosphate buffered saline (PBS) without stabilizing additives, indicating that it is highly stable.  
115 To corroborate the binding results with flow cytometry, S-transfected cells stained with saRBD1  
116 and AlexaFlor488-anti-VHH antibody were 30% VHH-positive by our gating scheme, while  
117 control VHH52 treated cells and un-transfected control cells were VHH-negative (Figure 1C).  
118 Together, our data indicate that saRBD-1 binds strongly to native SARS-CoV-2 S protein.



119

120 **Figure 1: A dominant VHH clone that binds SARS-CoV-2 spike, saRBD-1 was isolated**  
121 **from an alpaca immunized with RBD.** A) Schematic illustration of the immunization and VHH  
122 library construction pipeline. Alpacas were immunized over an 8-week period after which PBMC  
123 mRNA was isolated and processed into a VHH gene library. This library was transformed into  
124 phage-competent bacteria to generate a bacteriophage library, which was panned against  
125 SARS-CoV-2 S to enrich for binding clones. Clones were characterized through ELISAs on RBD  
126 and preliminary neutralization of S-pseudotyped lentivirus. B) Representative  
127 immunofluorescence staining showing saRBD-1 VHH specifically associates with SARS-CoV-2  
128 infected VeroE6 cells. Cells were infected with SARS-CoV-2 virus for 24 hours. Fixed cells were  
129 stained with either saRBD-1 or control VHH (VHH52) followed by anti-VHH secondary (green).  
130 SARS-CoV-2 infection indicated by anti-dsRNA which stains replication centers (red). C) SARS-  
131 CoV-2 S-transfected cells are specifically bound by saRBD-1 at levels detectable by flow  
132 cytometry. 293T cells transfected with full-length SARS-CoV-2 S were stained with either VHH  
133 saRBD-1 (green) or VHH52 (red) control.

134

135 **VHH saRBD-1 binds SARS-CoV-2 spike and receptor domain with high affinity**

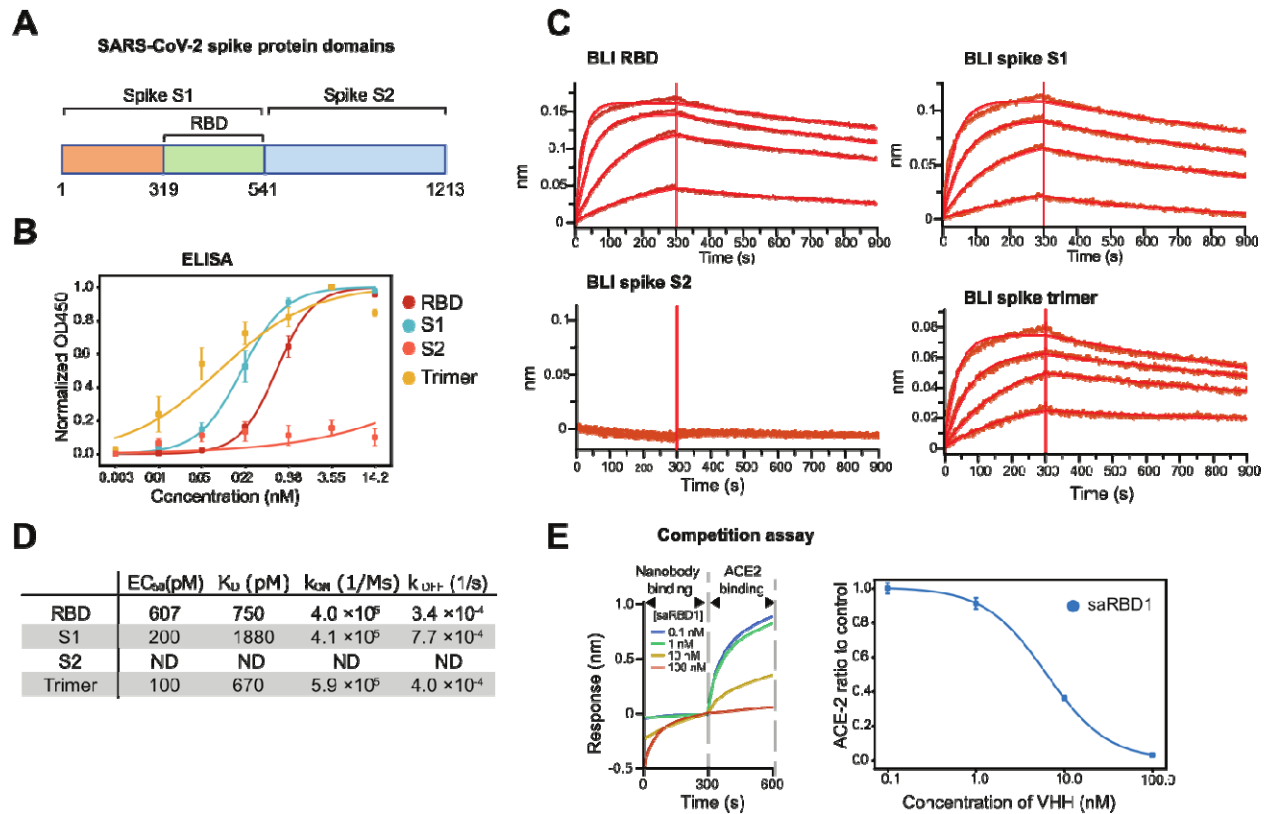
136 We determined the subunit specificity of saRBD-1 by ELISA on purified full-length trimeric S, S1  
137 (residues 14-684), RBD (residues 319-541), and S2 (residues 685-1273) proteins (Figure 2A).  
138 We found that saRBD-1 bound to full-length trimer with a 50% maximal binding response ( $EC_{50}$ )  
139 of 100 pM, to S1 with an  $EC_{50}$  of 200 pM, and to RBD with an  $EC_{50}$  of 607 pM, while S2  
140 showed no detectable binding, demonstrating that saRBD-1 binds specifically to the RBD  
141 subunit of the S protein (Figure 2B, D). Due to the promising initial binding characteristics of  
142 saRBD-1, we next investigated the binding kinetics in greater detail using bio-layer  
143 interferometry (BLI), which measures the effective mass change at the surface of a sensor tip.  
144 As expected, the S2 protein control yielded no binding (Figure 1C, D). However, BLI tips loaded  
145 with RBD measured a dissociation constant ( $K_D$ ) of 750 pM for saRBD1, while tips coated with  
146 S1 yielded a  $K_D$  1880 pM. S trimer loaded tips showed the strongest binding with a  $K_D$  of 674  
147 pM, consistent with our ELISA results. These  $K_D$ 's are lower than the previously reported 15 nM  
148  $K_D$  of the RBD-ACE2 interaction, suggesting that saRBD-1 binds SARS-CoV-2 with at least an  
149 order of magnitude greater affinity than ACE2 (Glasgow et al., 2020).

150

151 To more thoroughly examine this, we performed BLI-based competition assays to determine if  
152 saRBD-1 is able to block the RBD-ACE2 interaction (Figure 2E). In this assay, BLI tips were first  
153 loaded with RBD followed by varying concentrations of saRBD-1 VHH to block the RBD binding  
154 sites before finally transferring to a solution with a fixed concentration of ACE2. We found that  
155 saRBD-1 bound competitively with ACE2, and that a concentration of 6 nM of saRBD-1 was  
156 sufficient to block 50% of ACE2 binding. These results indicated that saRBD-1 binds specifically  
157 to the RBD subunit of native trimeric S protein with picomolar affinity and blocks the subsequent  
158 interaction of RBD with ACE2.

159





160

161 **Figure 2: VHH saRBD-1 binds SARS-CoV-2 spike and receptor domain with high affinity.**

162 A) Schematic identifying SARS-CoV-2 S protein domains. B) ELISA binding assay of saRBD-1

163 on plates coated with SARS-CoV-2 RBD, S1, S2, and full-length S trimer where saRBD-1 is

164 seen to bind RBD, S1, and full-length S trimer, but not S2. Curves show the average of 3

165 replicate experiments. C) Representative BLI curves of saRBD-1 binding kinetics experiments

166 on SARS-CoV-2 S RBD, S1, S2, and full-length trimer where saRBD-1 is seen to bind RBD, S1,

167 and full-length S trimer, but not S2. Biotinylated spike constructs were pre-bound to streptavidin

168 biosensor tips, after which association and dissociation steps were carried out in saRBD-1

169 solutions at (from top to bottom): 100nM, 31.6nM, 10nM, and 3.16nM. D) Summary data of

170 ELISA (B) and BLI (C) results. ELISA EC<sub>50</sub> values and BLI K<sub>D</sub>, k<sub>ON</sub> and k<sub>OFF</sub> values are the

171 average of at least two replicates. E) saRBD-1 competes with ACE2 receptor for binding SARS-

172 CoV-2 S RBD. ACE2 binding to RBD after blocking with different concentrations of saRBD-1 by

173 BLI. Resulting ACE2 binding values were by dividing by ACE2-only control. Left is

174 representative BLI trace and right is normalized ACE2 binding values fit to a dose-response  
175 curve, average of two replicates. Error bars in all plots represent standard error.

176

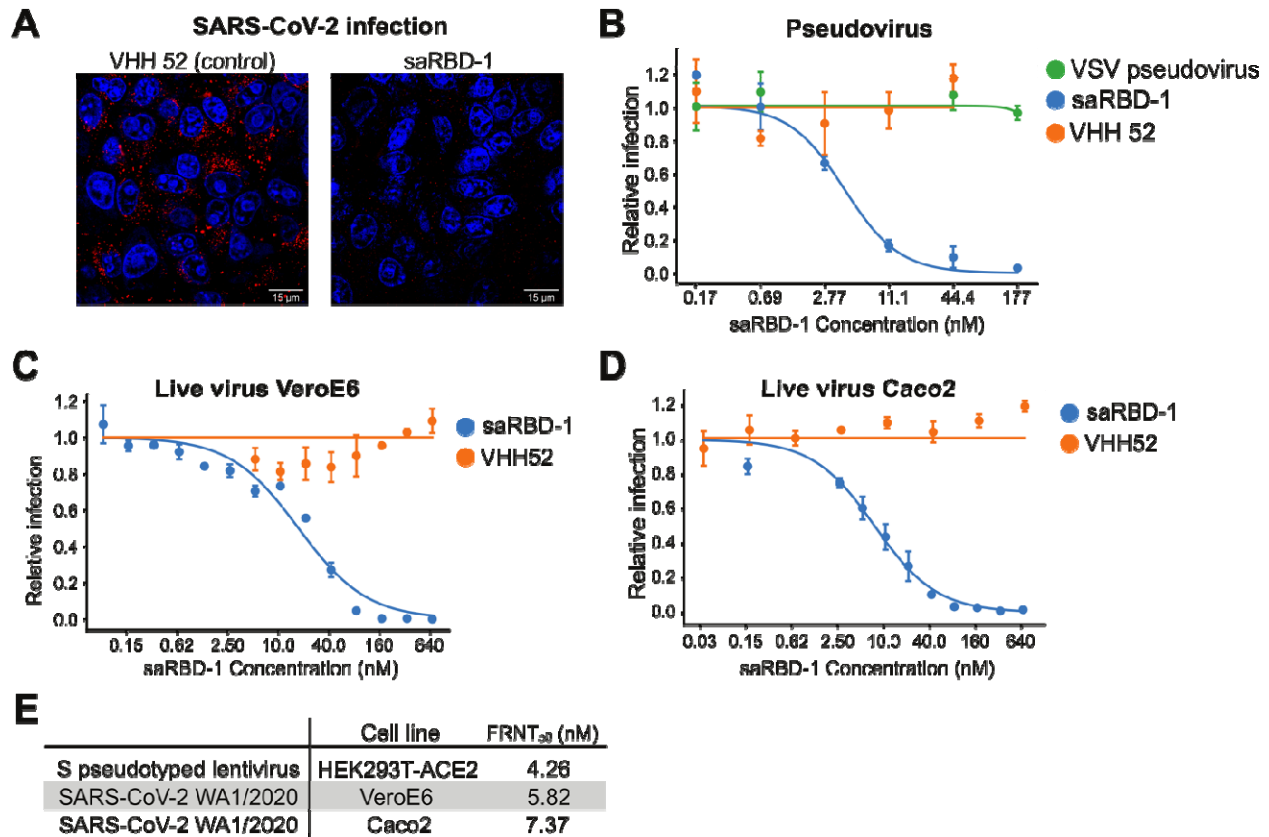
177 **VHH saRBD-1 neutralizes both SARS-CoV-2 spike-pseudotyped lentiviruses and live**  
178 **SARS-CoV-2 virions**

179 As an initial test of neutralization, we performed immunofluorescence microscopy on Vero E6  
180 cells infected in the presence of 179 nM of either saRBD-1, which we found to completely block  
181 infection, or 179 nM control VHH52 (Figure 3A). Infection was visualized with the anti-dsRNA  
182 antibody. To quantify the neutralizing potency of saRBD-1 we performed experiments for both  
183 pseudotyped virus and live SARS-CoV-2. For pseudotyped virus neutralization assays, GFP-  
184 bearing SARS-CoV-2 S pseudotyped lentivirus was incubated with dilutions of saRBD-1 or  
185 control VHH52 before being added to target 293T-ACE2 cells. Successful lentivirus transduction  
186 was detected by high-content fluorescence microscopy of GFP signals. The 50% inhibitory  
187 concentration ( $IC_{50}$ ) of the VHH for this lentivirus challenge was 4.26 nM (Figure 3B) while  
188 VHH52 showed no inhibition. To control for non-specific inhibition of lentivirus transduction,  
189 lentivirus was generated pseudotyped with the VSV G protein in lieu of SARS-CoV-2 S; VSV G  
190 pseudotyped virus was not neutralized by saRBD-1 (Figure 3B).

191

192 To determine VHH inhibitory activities against live SARS-CoV-2 virus, focus forming assays  
193 were performed using SARS-CoV-2 WA1/2020 strain and saRBD-1. For the assay, Vero E6 or  
194 human colorectal epithelial (Caco-2) cells were infected with SARS-CoV-2, then stained with  
195 anti-S alpaca polyclonal sera as a primary antibody and an HRP-conjugated secondary  
196 antibody, facilitating visualization of SARS-CoV-2 infected cells (Figure 3C, D). The 50% focus  
197 reduction neutralization titer ( $FRNT_{50}$ ) was found to be 5.82 nM for Vero E6, and 7.4 nM for  
198 Caco2 (Figure 3E). In comparison, the non-neutralizing VHH52 failed to decrease foci. Thus, it

199 is evident that monovalent saRBD-1 is a potent neutralizer of live SARS-CoV-2 *in vitro*, even at  
 200 low nanomolar concentrations.



201

202 **Figure 3: VHH saRBD-1 neutralizes both SARS-CoV-2 spike-pseudotyped lentiviruses**  
 203 **and live SARS-CoV-2 virions.** A) Representative images of assays used to quantify the effects  
 204 of saRBD-1 on viral entry. Representative microscopy of SARS-CoV-2 dsRNA (red) in presence  
 205 of 179 nM saRBD-1 or control VHH 52, cell nuclei stained with DAPI (blue). B) Neutralization of  
 206 S-pseudotyped lentivirus by saRBD-1. ACE2 positive HEK-293T cells were infected with GFP  
 207 reporter pseudovirus and either saRBD-1 or control VHH52. VSV G protein pseudovirus was  
 208 incubated with saRBD-1 similarly to S-pseudovirus. Cells were fixed after 48 hours, then stained  
 209 with DAPI and imaged. GFP signals were normalized to virus-only control wells. Averages of  
 210 three replicate experiments are shown. Neutralization of live SARS-CoV-2 virus by saRBD-  
 211 1 during infections of C) VeroE6 cells and D) Caco-2 cells. Neutralization was measured  
 212 by focus forming assay of live WA1/2020 pre-incubated with saRBD-1 or control VHH52. Data

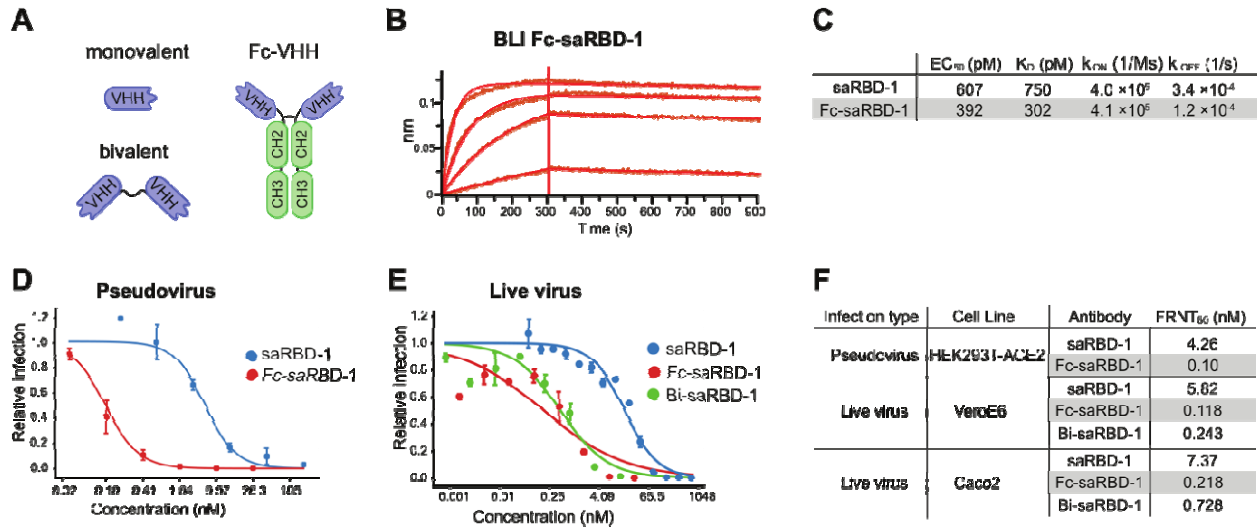
213 represent the average of at least two replicate experiments, each in technical triplicate. E)  
214 Summary table of 50% focus reduction neutralization (FRNT<sub>50</sub>) results from pseudovirus and  
215 live virus neutralization assays. Error bars in all plots represent standard error.

216

217 **An Fc conjugated bivalent VHH construct, and a dimeric saRBD-1 construct show**  
218 **improved binding and neutralization of SARS-CoV-2**

219 While monomeric saRBD-1 demonstrated exceptional neutralization of SARS-CoV-2, multimeric  
220 VHHs previously have been shown to have improved affinities and neutralization capabilities  
221 (Günaydın et al., 2016; Hanke et al., 2020; Schoof et al., 2020). To test this with saRBD-1, we  
222 utilized a mammalian vector to express saRBD-1 conjugated to human IgG Fc with a short  
223 hinge (Hanke et al., 2020; Tiller et al., 2008). The resulting chimeric protein is secreted as a  
224 dimer due to disulfide bridging of two Fc regions, and thus acts as a partially humanized heavy-  
225 chain only antibody (Figure 4A). This approach allows for improved binding due to avidity effects  
226 and greater steric blockage of the ACE2 binding site of the S protein. Simultaneously, we  
227 produced a bivalent construct of saRBD-1 (Bi-saRBD-1) attached by a flexible (GGGGS)<sub>4</sub> linker  
228 (Shan et al., 1999; Wrapp et al., 2020a). To determine binding kinetics of the saRBD-1 Fc-dimer  
229 (Fc-saRBD-1) to RBD, we utilized ELISA and BLI (Figure 4B-C, Figure S2). The EC<sub>50</sub> of Fc-  
230 saRBD-1 as measured by ELISA was 392 pM, a 50% stronger affinity as compared to  
231 monovalent saRBD-1. The K<sub>D</sub> of Fc-saRBD-1 as measured by BLI was 302 pM, primarily driven  
232 by a 3-fold reduction in the K<sub>OFF</sub> compared to monovalent saRBD-1. Using our pseudovirus  
233 neutralization assay, the neutralization ability of the Fc-saRBD-1 dimer improved to an IC<sub>50</sub> of  
234 100 pM, over a 40-fold improvement compared to monomeric saRBD-1 (Figure 4D, F).  
235 Neutralization of live SARS-CoV-2 by Fc-saRBD-1 had an FRNT<sub>50</sub> of 118 pM in VeroE6 cells  
236 and 218 pM in Caco2 cells, Bi-saRBD-1 had an FRNT<sub>50</sub> of 243 pM in VeroE6 cells and 728 pM  
237 in Caco2 cells. Compared to monomeric saRBD-1, this represents a 49-fold (Fc-saRBD-1) and  
238 24-fold (Bi-saRBD-1) improvement in neutralization on VeroE6 cells, and a 34-fold (Fc-saRBD-

239 1) and 10-fold (Bi-saRBD-1) improvement in Caco2 cells (Figure 4E, F). The slightly improved  
 240 neutralization shown by the Fc construct relative to the plain bivalent construct may be  
 241 explained by the increased steric hindrance from the bulky Fc portion (Hanke et al., 2020).



242

243 **Figure 4: An Fc conjugated bivalent VHH construct, and a dimeric saRBD-1 construct**  
 244 **show improved binding and neutralization of SARS-CoV-2.** A) Schematic of monovalent,  
 245 Fc-conjugated dimeric, and bivalent constructs. B) Representative BLI curves for Fc-saRBD-1  
 246 kinetic binding experiments on SARS-CoV-2 RBD. Biotinylated RBD was pre-bound to  
 247 streptavidin biosensor tips, after which association and dissociation steps were carried out in  
 248 saRBD-1 solutions at (from top to bottom): 100nM, 31.6nM, 10nM, and 3.16nM. C) Summary  
 249 table of BLI kinetic parameters. Data are the average of two replicates. D) SARS-CoV-2 S  
 250 pseudovirus neutralization curves showing the average of three microscopy experiments. E)  
 251 Live SARS-CoV-2 (WA1/2020) neutralization curves showing the average of at least (n=2)  
 252 replicate focus forming assay experiments, each in technical triplicate. F) Summary table of  
 253 FRNT<sub>50</sub> results from pseudovirus and live virus neutralization assays. Error bars in all plots  
 254 represent standard error.

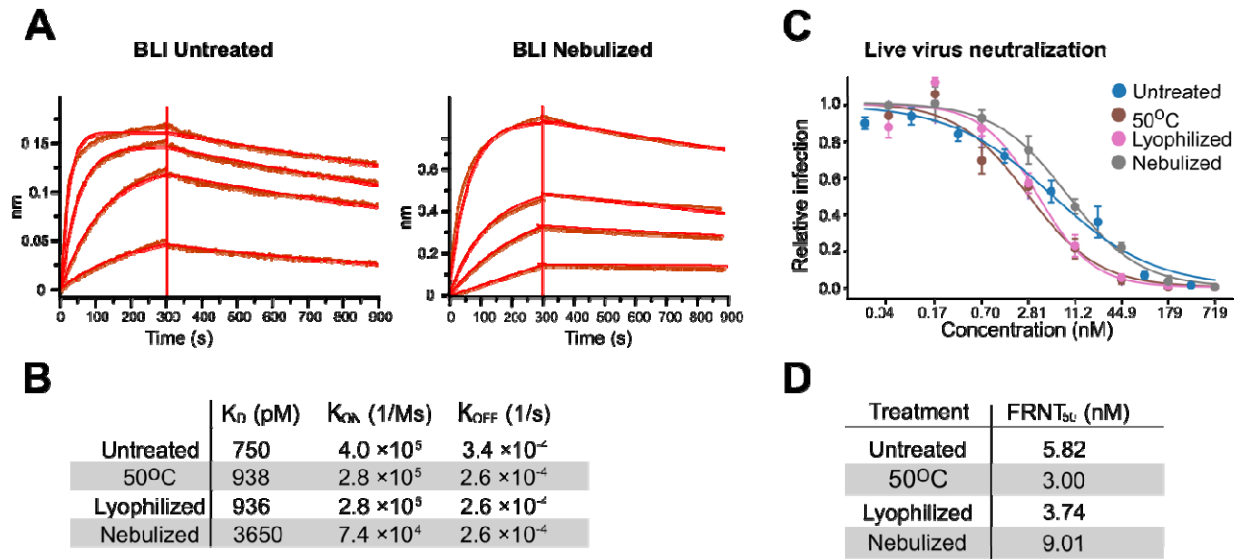
255

256

257 **saRBD-1 VHH is stable and maintains its activity after heat treatment, lyophilization and**  
258 **nebulization**

259 One of the major advantages of VHHs over conventional antibodies is their inherent stability.  
260 We evaluated the stability of saRBD-1 by subjecting it to some of the conditions that are likely to  
261 be encountered during production, transport, and delivery of protein-based therapeutics we  
262 evaluated the stability of saRBD-1 in elevated temperature, lyophilization, and nebulization. We  
263 treated VHH to each condition, then measured of protein loss, binding kinetics, and neutralizing  
264 ability of the treated VHH aliquots. Aliquots of saRBD-1 were incubated for 1 hour at 50°C then  
265 centrifuged to remove aggregates before measurement of protein loss by OD<sub>280</sub>, which showed  
266 a 19% reduction. The treated aliquots were then checked by BLI on RBD (Figure 5G, I), which  
267 showed minimal loss of activity concomitant with the reduction in measured protein  
268 concentration. Similar measurements were performed using lyophilized (29% protein loss) and  
269 nebulized (77% protein loss) samples. Nebulization is known to be a harsh process, particularly  
270 when performed in unmodified PBS solution with a jet nebulizer, and our numbers mirror  
271 previous reports of 4-fold loss of activity after nebulization with an ultrasonic nebulizer (Schoof  
272 et al., 2020). In total, we found that the K<sub>D</sub> was 938 pM for heat treatment, 936 pM for  
273 lyophilized, and 3.65 nM for aerosolized, amounting to 1.25-fold, 1.25-fold, and 4.8-fold  
274 increases respectively, which align with our protein loss determinations.

275  
276 To assay effects of these treatments on neutralizing activity, we carried out focus forming  
277 assays in VeroE6 cells utilizing the heat treated, lyophilized, and nebulized saRBD-1 samples  
278 (Figure 3H, J). We found that 50°C treated, lyophilized, and nebulized saRBD-1 yielded  
279 FRNT<sub>50s</sub> of 3.00 nM, 3.74 nM, and 9.01 nM respectively. In comparison, untreated saRBD-1  
280 yielded a FRNT<sub>50</sub> of 5.82 nM. Therefore, only nebulization reduced saRBD-1 neutralizing  
281 capability, with a 1.56-fold reduction. Overall saRBD-1 appears functionally stable, and it  
282 maintains nanomolar neutralization activity towards RBD even after destabilizing treatments.



283

284 **Figure 5: saRBD-1 VHH is stable and maintains its activity after heat treatment,**

285 **lyophilization and nebulization.** A) Representative BLI curves of kinetics experiments of

286 saRBD-1 binding RBD of untreated and nebulized samples. Biotinylated RBD was pre-bound to

287 streptavidin biosensor tips, after which association and dissociation steps were carried out in

288 saRBD-1 solutions at (from top to bottom): 100nM, 31.6nM, 10nM, and 3.16nM. B) Summary

289 table of BLI kinetics experiments of untreated, heat treated, lyophilized, and nebulized saRBD-1

290 samples. Data are the average of two replicates. C) Live SARS-CoV-2 focus forming assay

291 neutralization curves for untreated, heat treated, lyophilized, and nebulized saRBD-1 samples,

292 showing the average of at least two replicate experiments, each in technical triplicate.

293 E) Summary table of FRNT<sub>50</sub> results from live virus neutralization assays. Error bars in all plots

294 represent standard error.

295

296 **SaRBD-1 effectively neutralizes SARS-CoV-2 variants of concern**

297 Because of the prevalence of SARS-CoV-2 variant strains of concern (VOCs) significantly

298 divergent from the base strain (Figure 6A), we sought to test saRBD-1's affinity for mutated

299 RBD-N501Y and neutralizing abilities against clinical VOC isolates We generated a variant RBD

300 to test saRBD-1-RBD interactions. Using site directed mutagenesis, we created a spike and

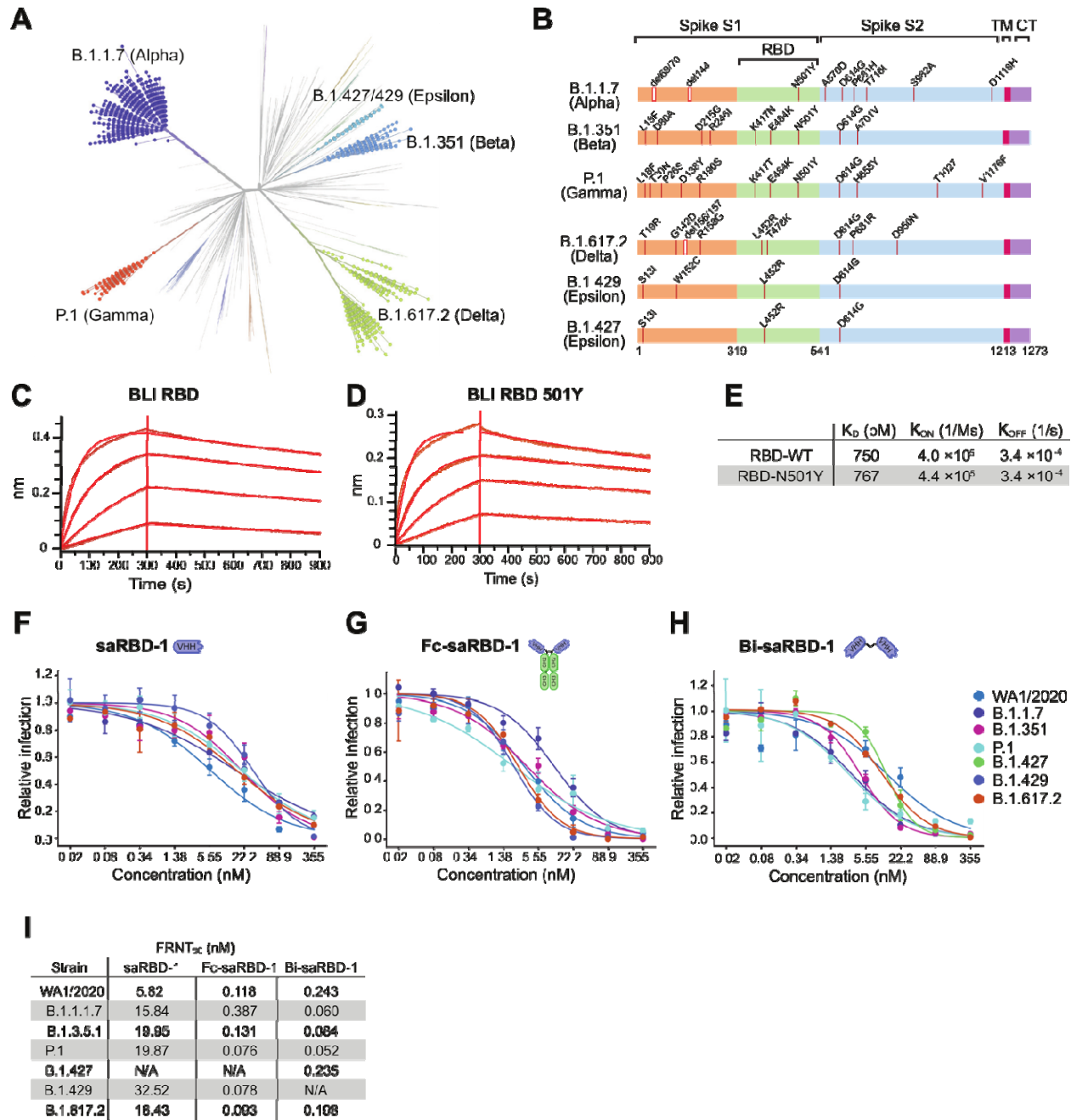
301 RBD variant that contained the N501Y mutation found in several of the circulating VOCs (Figure  
302 6B). Using BLI, we found binding of saRBD-1 to RBD-N501Y was similar to WT saRBD-1  
303 (Figure 6C, D), with a  $K_D$  of 767 pM compared to the WT value of 750 pM (Figure 6E). The  
304 affinity of saRBD-1 against both wild-type and mutant RBD constructs were stronger than the 15  
305 nM affinity of RBD for ACE2 (Glasgow et al., 2020), indicating that the N501Y amino acid  
306 change is unlikely to affect neutralization.

307

308 To more directly address variant cross-neutralization, we obtained clinical isolates of the  
309 following SARS-CoV-2 VOCs with known RBD mutations: Alpha containing N501Y; Beta  
310 containing K417N, E484K, N501Y; Gamma containing K417T, E484K, N501Y; Epsilon  
311 containing L452R; and Delta containing RBD L452R and T478K. Compared to the FRNT<sub>50</sub> of  
312 5.82 nM on WA1/2020, the variants were neutralized with FRNT<sub>50</sub> values of 15.84 nM (Alpha),  
313 19.95 nM (Beta), 19.87 nM (Gamma), 32.52 nM (Epsilon), and 16.43 nM (Delta), representing  
314 3-fold to 6-fold reductions that may be due to marginal differences in binding or natural  
315 experimental variation in the focus forming assays (Figure 6F-I). We additionally sought to test  
316 the efficacy of our Fc-conjugated VHH against all VOCs. We found FRNT<sub>50</sub>'s of 118 pM  
317 (WA1/2020), 387 pM (Alpha), 131 pM (Beta), 76 pM (Gamma), 78 pM (Epsilon), and 93 pM  
318 (Delta), which are all within 3-fold of WA1/2020 (Figure 6I). Finally, we utilized our Bi-saRBD-1  
319 construct for VOC neutralization assays. With this construct, we found FRNT<sub>50</sub>'s of 243 pM  
320 (WA1/2020), 60 pM (Alpha), 56 pM (Beta), 235 pM (Gamma), 198 pM (Delta), where all variants  
321 are better neutralized than WA1/2020. Overall, our monomer saRBD-1 displayed low nanomolar  
322 FRNT<sub>50</sub>'s against all VOCs, while our dimeric constructs retained picomolar levels. Therefore,  
323 saRBD-1 likely targets an RBD epitope that is conserved across all tested SARS-CoV-2 VOCs.

324





325

326 **Figure 6: SaRBD-1 effectively neutralizes SARS-CoV-2 variants of concern. A)**

327 Phylogenetic tree including the VOCs. The tree was generated in Nextstrain of all available

328 variants with the VOCs used in this study highlighted and labeled. B) Schematic diagram of the

329 variant spike protein amino acid changes present in the VOCs. Representative BLI curves of

330 kinetic experiments of saRBD-1 on C) RBD and D) RBD-N501Y. Biotinylated RBD and RBD-

331 N501Y were pre-bound to streptavidin biosensor tips, after which association and dissociation

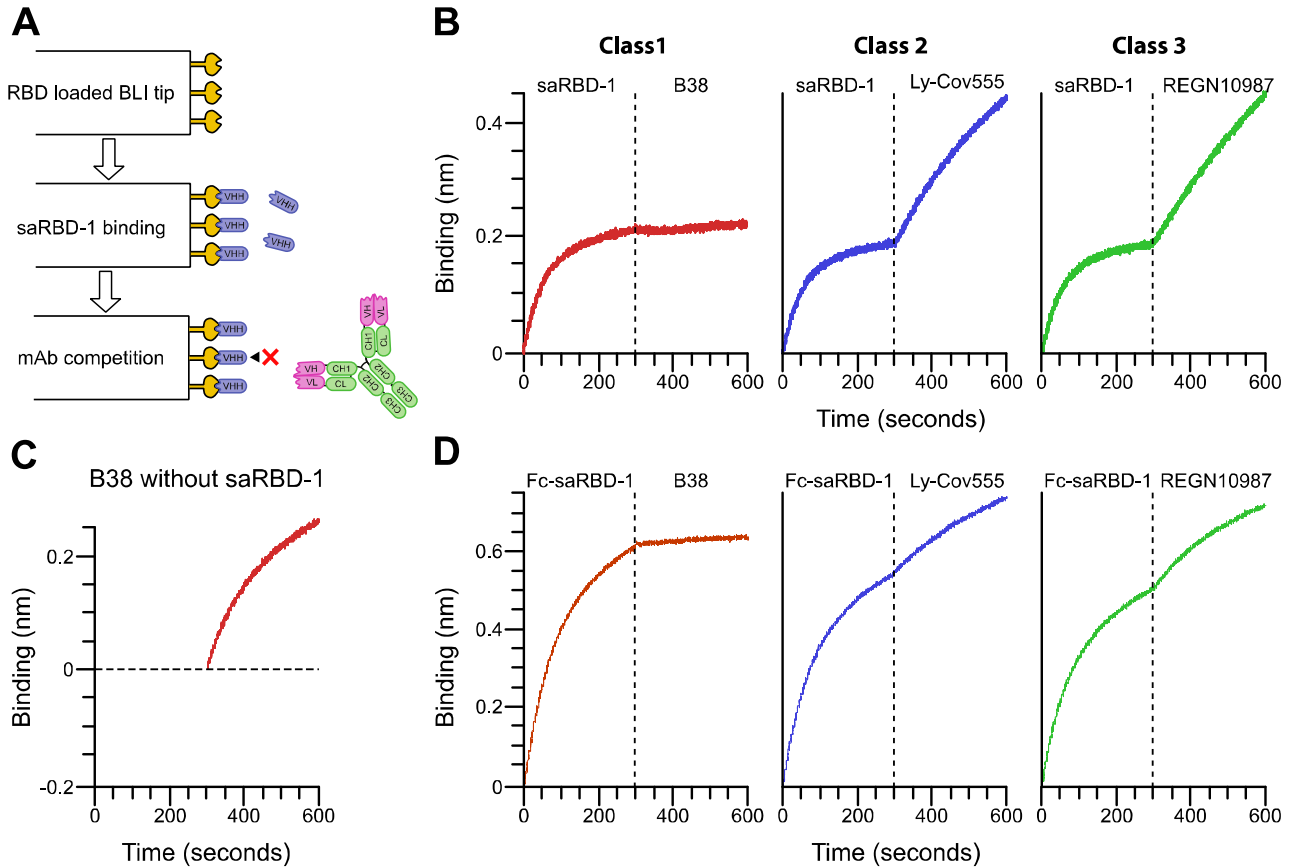
332 steps were carried out in saRBD-1 solutions at (from top to bottom): 100nM, 31.6nM, 10nM, and  
333 3.16nM. E) Summary table of binding kinetic values of saRBD-1 on RBD and RBD-N501Y,  
334 determined by BLI. Data are the average of two replicates. Live SARS-CoV-2 focus forming  
335 assay neutralization curves of the VOCs for F) monomeric saRBD-1, G) dimeric Fc-saRBD-1,  
336 and H) bivalent Bi-saRBD-1. Data are the average of two replicate experiments, each in  
337 technical triplicate. I) Summary table of FRNT<sub>50</sub> results from live virus neutralization assays.  
338 N/A: Not tested. Error bars in all plots represent standard error.

339

### 340 **SaRBD-1 competes with class-1 monoclonal antibody B38**

341 To narrow down the binding epitope of saRBD-1, we performed competitive binding assays  
342 against monoclonal antibodies from the three primary classes of RBD binding antibodies (Figure  
343 7A). Class 1 antibodies bind epitopes around K417 and tend to bind spike in the up  
344 conformation, while class 2 antibodies bind epitopes around E484 and can bind both up and  
345 down conformations, and class 3 antibodies bind epitopes around L452, distal to the ACE2  
346 contact surface (Barnes et al., 2020). We selected representative antibodies from each class:  
347 class 1: B38 (Wu et al., 2020), class 2: Ly-Cov555 (Greaney et al., 2021; Jones et al., 2021),  
348 class 3: REGN10987 (Greaney et al., 2021; Weinreich et al., 2021) to use in a biolayer  
349 interferometry (BLI) competitive binding assay. In this assay, SARS-CoV-2 spike RBD protein  
350 was attached to a sensor and first exposed to saRBD-1, which bound strongly during the first  
351 300 seconds. In the subsequent step, the sensors were transferred to solutions containing the  
352 representative monoclonal antibodies. SaRBD-1 successfully blocked B38 from binding,  
353 indicating that they likely bind to overlapping epitopes (Figure 7B). The class 2 & 3 antibodies  
354 were not affected by saRBD-1. A control experiment confirmed that B38 binds successfully  
355 when saRBD-1 was absent (Figure 7C). These results were recapitulated with a dimeric Fc-  
356 saRBD-1 construct (Figure 7D). Hence, saRBD-1 is most likely a class 1 binder. An unlikely

357 alternative is that saRBD-1 binds a distal site non-competitive with the class 3 antibody, but  
358 forces RBD into a down conformation unsuitable for B38 binding.



359  
360

361 **Figure 7: saRBD-1 competes with class-1 monoclonal antibody B38.** A) Experimental  
362 design of BLI-based competition assay of monoclonal antibodies. B) BLI measurement of  
363 saRBD-1 binding followed by class 1, 2, or 3 monoclonal antibodies. Binding. B38 (class 1) is  
364 shown in red, LyCoV-555 (class 2) is in blue, and REGN19087 (class 3) is in green. C) BLI  
365 measurement of B38 (class 1) binding in the absence of saRBD-1. D) BLI measurement of Fc-  
366 saRBD-1 binding followed by class 1, 2, or 3 monoclonal antibodies.

367

368 **Discussion**

369 The ongoing SARS-CoV-2 pandemic is a threat to global public health; the discovery and  
370 synthesis of additional therapeutics and vaccines are needed to address this. Although the  
371 scientific community has developed effective vaccines (Baden et al., 2021; Daniel et al., 2021;  
372 Shen et al., 2021) against the initial SARS-CoV-2 outbreak, ongoing concern that a vaccine  
373 resistant VOC could result in a resurgent outbreak has played out with the arrival of the Omicron  
374 VOC (Liu et al., 2021c; Zhang et al., 2021). Two of the most widely utilized vaccine options from  
375 Pfizer/BioNTech and Moderna, are expensive and unstable mRNA vaccines, requiring  
376 specialized transportation and storage (Crommelin et al., 2021; Kartoglu et al., 2020). This has  
377 resulted in a dearth in vaccine availability for communities around the world compounding the  
378 human impact of the SARS-CoV-2 pandemic and transmission of VOCs (Holder; Mathieu et al.,  
379 2021). Increasing evidence also points to waning immune responses to the vaccines, increasing  
380 the risk of breakthrough infections (Levin et al., 2021; Shrotri et al., 2021) As such, novel  
381 therapeutics and vaccines should fulfill both the following conditions: 1) be affordable to  
382 produce, transport and store. 2) provide highly effective long-term protection against circulating  
383 VOCs. Our saRBD-1 VHH is an ideal match due to its cheap manufacture of bacterial  
384 purification, thermostability, and efficacy at VOC neutralization.

385

386 The ability of saRBD-1 to potently neutralize SARS-CoV-2 is critical to its potential. Antiviral  
387 VHHs have utility as prophylactics or therapeutics against viral infections (Ingram et al., 2018;  
388 Laursen et al., 2018). Hence, strongly neutralizing VHHs against SARS-CoV-2 are desirable.  
389 Other groups have isolated VHH candidates that bind S RBD and neutralize SARS-CoV-2  
390 infections in situ (Güttler et al., 2021; Hanke et al., 2020, 2022, 2022; Koenig et al., 2021;  
391 Schoof et al., 2020; Wagner et al., 2021; Wrapp et al., 2020a; Xiang et al., 2020; Xu et al.,  
392 2021) and in animal models (Kim et al., 2021; Pymm et al., 2021; Wagner et al., 2021). The  
393 monomeric form of saRBD-1 potently neutralizes ancestral SARS-CoV-2 and VOCs with

394 FRNT<sub>50</sub> of around 5.82 nM. Other VHHs within a similar range of neutralizing potency have been  
395 reported (Pymm et al., 2021; Xu et al., 2021). Strong inhibition of SARS-CoV-2 is critical for  
396 VHH therapeutic potential, as the highest possible neutralizing strength is ideal for minimizing  
397 the effective dose of a potential treatment. Another encouraging quality of saRBD-1 is its  
398 extreme stability against multiple forms of insult. SaRBD-1 retained neutralizing activity and  
399 RBD- binding capability when heated to 50°C, nebulized or lyophilized. These tests are relevant  
400 because they mimic the likely transport, storage, and delivery conditions that are likely to be  
401 encountered by a therapeutic anti-SARS-CoV-2 nanobody.

402

403 As a bivalent construct or when conjugated to a human IgG Fc domain, saRBD-1 has  
404 comparable neutralizing capabilities to highly neutralizing monoclonal antibodies, reaching ~100  
405 pM FRNT<sub>50</sub>s against live SARS-CoV-2. As such, Bi-saRBD-1 and Fc-saRBD-1 may prove  
406 useful for prophylaxis in a similar manner to convalescent plasma transfusions, which have had  
407 positive clinical outcomes throughout the COVID-19 pandemic (Hu et al., 2020; Zeng et al.,  
408 2020). Although the addition of the Fc domain to nanobodies undermines the key beneficial  
409 features of small size and may cause antibody-dependent enhancement (Eroshenko et al.,  
410 2020), Fc-conjugation is known to significantly increase the in vivo half-life of nanobodies  
411 (Rotman et al., 2015).

412

413 The most appealing characteristic of saRBD-1 is its activity against SARS-CoV-2 VOCs. VOCs  
414 pose a global threat beyond that of the initial SARS-CoV-2 pandemic, as such effective  
415 treatments are especially valuable to protecting public health. VOCs tend to have increased  
416 transmission compared to the initial pandemic strains of SARS-CoV-2 (Chen et al., 2021;  
417 Korber et al., 2020; Liu et al., 2021a). Furthermore, VOCs with multiple S protein RBD  
418 mutations resist neutralization by vaccinated sera and convalescent patient sera (Bates et al.,  
419 2022; Chen et al., 2021; Liu et al., 2021c). Development of VOCs increases the possibility of

420 new mutations developing that escape vaccination, especially with partial vaccination of global  
421 population or waning antibody levels in those vaccinated (Levin et al., 2021; Mathieu et al.,  
422 2021; Shrotri et al., 2021). Although several VHHs are reported with neutralizing activities  
423 against Alpha (Pymm et al., 2021; Zupancic et al., 2021) and Beta (Güttler et al., 2021; Hanke  
424 et al., 2022; Mast et al., 2021; Wagner et al., 2021; Xu et al., 2021; Zupancic et al., 2021), few  
425 are published with activity against Gamma (Mast et al., 2021) and Delta (Wagner et al., 2021).  
426 Previous studies have reported that combinations of neutralizing VHHs delivered *in-situ* SARS-  
427 CoV-2 infections are important to suppress development of escape mutations (Wrapp et al.,  
428 2020a) and better neutralize variant strains (Pymm et al., 2021). A great variety of VOC  
429 neutralizing VHHs will be crucial if nanobodies are to play a role as SARS-CoV-2 therapeutics  
430 against future evasive VOCs similar to Omicron. Thus saRBD-1 can be valuable due to its  
431 proven ability to neutralize 5 distinct VOC strains, including Delta.

432  
433 Neutralizing antibodies against SARS-CoV-2 RBD can be organized into three classes  
434 depending on their targets in the RBD-ACE2 interface and confirmation of RBD when binding.  
435 Class 1 binds up RBD at the ACE2 binding site, class 2 binds up and down RBD at the ACE2  
436 binding site, and class 3 binds up and down through residues distal to the ACE2-binding site  
437 (Barnes et al., 2020). Therefore, class 1 and 2 antibodies target RBD residues that are  
438 frequently mutated in VOCs such as K417, E484 and N501; L452 is the most commonly  
439 mutated residue bound by class 3 antibodies (Greaney et al., 2021). Among the published  
440 VHHs, Fu2 (Hanke et al., 2022) and WNb2 (Pymm et al., 2021) appear to be class 1, while Nb6  
441 and Nb11 (Schoof et al., 2020), Nb20 (Xiang et al., 2020) and Ty1 (Hanke et al., 2020) are class  
442 2. Class 3 nanobodies are also reported, including WNb10 and 15 (Pymm et al., 2021), Nb12  
443 and Nb30 (Xu et al., 2021), and VHH72 (Wrapp et al., 2020a). We determined that saRBD-1  
444 belongs to class 1 due to competition with class 1 monoclonal antibody B38 (Wu et al., 2020).

445 Interestingly, saRBD-1 neutralizes VOCs containing K417, E484, and N501 mutations that  
446 typically affect class 1 and 2 antibodies, suggesting its epitope identity or mechanism of  
447 neutralization may be atypical for class 1 neutralizing antibodies. The recently published VHH  
448 Fu2 is an example of an atypical mechanism of SARS-CoV-2 neutralization (Hanke et al.,  
449 2022). Fu2 binds as a class 1 antibody to block ACE2 binding to RBD, yet simultaneously  
450 induces dimerization in full-length spike to further disrupt ACE2 interactions. Fu2 was also found  
451 to neutralize the Beta variant without significant loss of potency. Thus, a VHH may have  
452 unexpected levels of utility outside of those predicted by epitope class, which can aid in binding  
453 mutated RBD variants.

454

455 We found that saRBD-1 binds competitively with human ACE2 for SARS-CoV-2 spike RBD, and  
456 that pre-incubation of RBD with saRBD1 blocks ACE2 binding, a necessary step to infection.  
457 Low nanomolar concentrations of monovalent saRBD-1 successfully neutralize clinical isolates  
458 of the Alpha, Beta, Gamma, Epsilon, and Delta VOC as a likely class 1 antibody. Both the Bi-  
459 saRBD-1 and Fc-saRBD-1 demonstrate improved binding, and they successfully neutralize the  
460 variants at picomolar concentrations with no discernable loss of potency. Due to its high  
461 neutralizing efficacy, saRBD-1, alone or in combination with other ultra-potent VHHs, is an  
462 excellent candidate for development into a therapeutic to manage severe COVID-19.

463

## 464 **Methods**

### 465 **Key resource table**

REAGENT or RESOURCE	SOURCE	IDENTIFIER
Antibodies		
Anti-VHH biotin	Jackson	128-065-232
Streptavidin-HRP	ThermoFisher	N100

mouse anti-dsRNA	Millipore Sigma	MABE1134
Anti-mouse IgG AF555	Abcam	ab150114
anti-VHH Alexa Fluor 488	Jackson	2810926
Anti-llama IgG FITC	ThermoFisher	A16061
Anti-VHH-HRP	Jackson	2810909
SARS-CoV-2 Spike RBD monoclonal mouse IgG2a antibody (Clone B38)	Wu et al., 2020, Invivogen	cov2rbdc2-mab10
Recombinant monoclonal mouse IgG2a (Imdevimab-derived)	Weinreich et al., 2021, Invivogen	srbdc4-mab10
Recombinant monoclonal mouse IgG2a (Bamlanivimab-derived)	Jones et al., 2021, Invivogen	srbdc5-mab10
Bacterial and virus strains		
TG1 Electroporation-Competent Cells	Agilent	200123
<i>E. Coli</i> K12 ER2738	NEB	E4104
SARS-CoV-2 WA1/2020	BEI Resources	NR-52281
SARS-CoV-2 B.1.1.7	BEI Resources	NR-54011
SARS-CoV-2 B.1.351	BEI Resources	NR-54009
SARS-CoV-2 P.1	BEI Resources	NR-54982
SARS-CoV-2 B.1.427	BEI Resources	NR-55308
SARS-CoV-2 B.1.429	BEI Resources	NR-55309
SARS-CoV-2 B.1.617.2	BEI Resources	NR-55611
Biological samples		
Spike immunized whole alpaca blood	Capralogics Inc.	N/A
Chemicals, peptides, and recombinant proteins		
TMB substrate solution	ThermoFisher	N301
Lipofectamine 3000	ThermoFisher	L3000015
phalloidin-Alexa Fluor 488	ThermoFisher	A12379
streptavidin-AF488	Jackson	016-540-084



SYPRO Orange 5000x	ThermoFisher	S6650
Purified SARS-COV-2 RBD	BEI	NR-52306
Purified SARS-CoV-2 spike S1	BEI	NR-53798
Purified SARS-CoV-2 spike S2	BEI	NR-53799
Purified SARS-CoV-2 full length spike trimer	BEI	NR-52396
Critical commercial assays		
ChromaLINK biotin protein labeling kit	Vector labs	B-9007-105K
RNeasy Mini Kit	Qiagen	74104
Experimental models: Cell lines		
HEK-293T-ACE2	Dr. Jesse Bloom (UW)	NR-52511
HEK-293T	ATCC	CRL-3216
Vero E6	ATCC	CRL-1586
Caco2	ATCC	HTB-37
HEK-293-F	Gibco	R79007
Oligonucleotides		
Immunoglobulin cDNA primer 1: ATGGAGAGGACGTCCTTGGGT	Maass et al. 2007	N/A
Immunoglobulin cDNA primer 2: TTCGGGGGGAAGAYRAAGAC	Maass et al. 2007	N/A
VHH universal forward amplification primer: GATCGCCGCCAGKTGCAGCTCGTGGAGTCNGGN GG	Maass et al. 2007	N/A
VHH long hinge reverse primer: GATCACTAGTGGGGTCTTCGCTGTGGTGCG	Maass et al. 2007	N/A
VHH short hinge reverse primer: GATCACTAGTTTGTGGTTTTGGTGTCTTGGG	Maass et al. 2007	N/A
Recombinant DNA		
pLVX-IRES-Puro vector	Takara Bio	632183

pTwist-EF1alpha-nCoV-2019-S-2xStrep	Gordon et al. 2020, Krogon Lab, BEI Resources	10.5281/zenodo.37 79045
HDM_IDTSpike_fixK, SARS-CoV-2 plasmid	Crawford et al. 2020 , Bloom lab, BEI Resources	NR-52514
HDM_Hgpm2	Crawford et al. 2020 , Bloom lab, BEI Resources	NR-52517
HDM_tat1b	Crawford et al. 2020 , Bloom lab, BEI Resources	NR-52518
pRC_CMV_Rev1b	Crawford et al. 2020 , Bloom lab, BEI Resources	NR-52519
pHAGE2_CMV_ZsGreen_W	Crawford et al. 2020 , Bloom lab, BEI Resources	NR-52520
Software and algorithms		
BZ-X700 Analyzer Microscope software	Keyence	v1.4
Immunospot analyzer	CTL	v5.3
Viridot focus counting package for R	Katzelnick et al., 2018	v1.0
R	R project	v4.1.0
Python	Python Software Foundation	v3.8.10
Dose response calculator	Bates et al., 2021	10.5281/zenodo.51 58655
Other		
Streptavidin biosensors	Sartorius	18-5019

466

467 **Experimental model and subject details**

468 HEK-293T stable cell lines expressing human ACE2 receptor (HEK-293T-ACE2) were a kind

469 gift from Dr. Jesse D. Bloom from University of Washington, and described previously (Crawford

470 et al., 2020). Low-passage HEK-293T, HEK-293T-ACE2, and Vero E6 cells were cultured in  
471 D10, which consisted of Dulbecco's Modified Eagle Medium (DMEM) supplemented with 10%  
472 fetal bovine serum (FBS), 1% Penn-Strep, 1% non-essential amino acids (NEAA). 37°C. Caco2  
473 cells were cultured in D20 (D10 with 20% FBS instead of 10%). Cells were cultured in T75  
474 dishes, passaged with Trypsin at 95% confluency to avoid overcrowding.

475

#### 476 **RBD protein purification and biotinylation**

477 Purified SARS-CoV-2 S-RBD protein was prepared as described previously (Amanat et al.,  
478 2020). Briefly, codon optimized his-tagged RBD or RBD containing the N501Y mutation in  
479 pLVX-IRES-puro plasmid (Takara Bio) was used to make lentivirus vectors in HEK-293T cells,  
480 which were then used to infect HEK-293F suspension cells. The suspension cells were grown in  
481 FreeStyle™ 293 expression medium (Gibco) for 3 days with shaking at 37°C with 8% CO<sub>2</sub>. Cell  
482 supernatants were collected, sterile filtered, and purified by Ni-NTA chromatography (Bierig et  
483 al., 2020). Purified protein was then buffer exchanged into phosphate-buffered saline (PBS) by  
484 dialysis and concentrated with 10kDa cutoff centrifuge filters (Millipore). For use in BLI, purified  
485 RBD was biotinylated using the ChromaLINK biotin protein labeling kit (Vector) according to the  
486 manufacturer's instructions with 5x molar equivalents of labeling reagent to achieve 1.92  
487 biotins/protein.

488

#### 489 **VHH gene library construction**

490 Alpacas were immunized at Capralogics Incorporate (Hardwick, MA). Animals received three  
491 immunizations of 1 mg purified SARS-CoV-2 RBD spaced three weeks apart. Blood was  
492 harvested 5 days after third immunization. Upon receipt PBMCs were isolated (Eppendorf) and  
493 used in an RNA extraction with Qiagen RNeasy mini kit (Qiagen). PBMC RNA, containing VHH  
494 genes, was converted into cDNA using Superscript III reverse transcriptase (Invitrogen). VHH  
495 genes were amplified with custom primers specific to short-hinge and long hinge VHH genes

496 appended with Not1 and Asc1 restriction sites (Maass et al., 2007; Schmidt, 2018). The  
497 amplified gene mixture was cloned into a phage-mid plasmid derived from pCANTA5BE, then  
498 transformed via electroporation into bacteriophage competent TG1 Escherichia coli for  
499 production of a VHH displaying bacteriophage library. The pooled library was rescued at 37°C  
500 with shaking and plated. Plates containing serial dilutions were used to estimate total bacterial  
501 population, and therefore library diversity. A representative sample of 96 VHH clones were sent  
502 for sanger sequencing (Genewiz) to confirm VHH diversity.

503

#### 504 **VHH panning**

505 M13-derived helper phage were produced through standard protocols (Frei and Lai, 2016). VHH  
506 libraries in TG1 cells were transduced with helper phage to produce bacteriophage displaying  
507 individual VHHs. Phage were isolated through precipitation using 20% w/v polyethylene glycol  
508 8000, then were resuspended in PBS. Phage libraries were then panned against full length  
509 stabilized SARS-CoV-2 spike protein trimer BEI resources NR-52396 at 10ug/ml alongside BSA  
510 controls. Bacteriophage were bound to the antigen, washed, then eluted with 200mM glycine pH  
511 2.2, neutralized with 1M Tris pH 9.1, and transduced into ER2738 bacteriophage competent  
512 bacteria which were plated on antibiotic agar and incubated for 18 hours at 37°C. Panning  
513 success was determined by enrichment 10-fold greater total bacterial colonies above control  
514 panning background. Panning colonies were then pooled, and the protocol was repeated for 2<sup>nd</sup>  
515 round panning using 2ug/ml antigen coating. A selection of colonies from 2<sup>nd</sup> round panning  
516 were picked and grown up in 96 deep-well plates for screening.

517

#### 518 **Screening of VHH candidates**

519 96 well ELISAs coated with 1ug/ml purified RBD were used to determine RBD binding affinities  
520 of panning hits. ELISAs were ran with bacterial supernatant containing secreted VHHs as  
521 primary antibody, then anti-nanobody biotin antibody (Jackson #128-065-232) and streptavidin-

522 HRP antibody (Thermo #N100) were used as secondary. 3,3', 5'5"-tetramethylbenzidine (TMB)  
523 (ThermoFisher Scientific) was used as peroxidase substrate, 50  $\mu$ l added for 10 minutes at  
524 room temperature (RT) then 50  $\mu$ l of 2N H<sub>2</sub>SO<sub>4</sub> was added as a stopping solution. Plate  
525 absorbance at 405 nm was measured using a CLARIOstar® Plus plate fluorimeter (BMG  
526 Labtech). VHH candidates with binding greater than 2-fold above average background were  
527 picked and sent for sanger sequencing (Genewiz) to identify VHH CDR3 regions. Clones that  
528 appeared multiple times in sequencing were cloned into a periplasmic expression vector (pHEN)  
529 by Gibson assembly. Bacteria were grown up in terrific broth (2% tryptone, 1% yeast extract,  
530 90mM phosphate), induced with isopropylthio- $\beta$ -galactoside (IPTG) at 30°C overnight. VHHS  
531 were isolated by osmotic shock (Saerens et al., 2004) , periplasmic fraction was isolated, and  
532 his-tagged VHHS were purified with Ni-NTA chromatography. Purified VHH was then buffer  
533 exchanged and concentrated with 3kDa cutoff centrifuge filters (Millipore), then filter sterilized by  
534 22  $\mu$ m centrifugal sterile filter (Millipore Sigma) prior to use in experiments.

535

### 536 **Multivalent saRBD-1 construction and purification**

537 Fc-conjugated (Hanke et al., 2020) and bivalent saRBD-1 (Wrapp et al., 2020b) constructs were  
538 synthesized using guidance from prior publications. Fc-saRBD-1 gene was directly synthesized  
539 containing an sp6 promotor, secretion signal, saRBD-1, flexible hinge, human IgG1 Fc region  
540 (Tiller et al., 2008), and 6x his tags for cloning into pLVX-IRES-puro plasmid (Takara Bio).  
541 Lentivirus encoding Fc-saRBD-1 was produced, and protein was purified from transduced 293F  
542 cells as described for RBD purification above. Fc-saRBD-1 was then further purified by ion-  
543 exchange chromatography for a final yield of ~4.6 mg per 100 ml of initial supernatant. Bivalent-  
544 saRBD-1 gene was synthesized containing two saRBD-1 genes separated by a flexible 20 a.a  
545 (GGGGS)<sub>4</sub> linker, for cloning into pET24a bacterial expression plasmid. Bacteria were grown in  
546 terrific broth (2% tryptone, 1% yeast extract, 90mM phosphate), induced with isopropylthio- $\beta$ -  
547 galactoside (IPTG) at 30°C overnight, lysed in Tris-NaCl buffer (500mM NaCl 20mM Tris, pH 8)

548 by sonication and purified by Ni-NTA chromatography. Both multivalent proteins were buffer  
549 exchanged to remove excess imidazole and concentrated with 10 kDa cutoff centrifuge filters  
550 (Millipore), then filter sterilized by 22  $\mu$ m centrifugal sterile filter (Millipore Sigma) prior to use in  
551 experiments.

552

### 553 **Cell transfection**

554 HEK-293T cells seeded at 70-90% cell density, then transfected using Lipofectamine 3000  
555 (ThermoFisher Scientific) as per manufacturer's instructions. For S transfection, the SARS-  
556 CoV2 structural protein plasmid pTwist-EF1alpha-nCoV-2019-S-2xStrep a kind gift from the  
557 Krogan lab at UCSF, was used as described previously (Gordon et al., 2020). For pseudotyped  
558 lentivirus production, the following reporter plasmids and lentivirus packaging plasmids were  
559 used as described previously (Crawford et al., 2020): HDM\_Hgpm2, HDM\_tat1b,  
560 PRC\_CMV\_Rev1b packaging plasmids, SARS\_CoV-2 S plasmid HDM\_IDTSpike\_fixK, and  
561 LzGreen GFP- reporter plasmid. Packaging, SARS-CoV-2 S, and reporter plasmids were a kind  
562 gift from the Bloom Lab at University of Washington. Per 6 well plate, 0.44  $\mu$ g of each,  
563 packaging plasmid, 0.68  $\mu$ g of S, and 2  $\mu$ g of reporter plasmids were used for transfection. For  
564 all transfections, media was carefully removed 6 hours post transfection, and replaced with D10.

565

### 566 **SARS-CoV-2 virus propagation**

567 Clinical isolates of SARS-CoV-2 variants were obtained from BEI resources: WA1/2020 (NR-  
568 52281), Alpha (NR-54011), Beta (NR-54009), Gamma (NR-54982), Epsilon (NR-55308) and  
569 (NR-55309), Delta (NR-55611). To propagate, a 70% confluent T25 flask of Vero E6 cells was  
570 infected at a MOI of 0.01 in diluted in 1 mL Opti-MEM for 1 hour at 37°C with occasional  
571 rocking. 4mL of D10 was then added and the flask was incubated for 72 hours at 37°C.  
572 Following incubation, flasks were checked for cytopathic effect (CPE), after which supernatant  
573 was collected and spun at 3000xg for 5 minutes to remove cellular debris, then aliquoted for

574 storage at -80°C. Propagated stocks were titrated with 8 × 10-fold dilutions in a focus forming  
575 assay as described below.

576

### 577 **SARS-CoV-2 immunofluorescence**

578 96-well TC plates were seeded to 50% confluency with VeroE6 or Caco2 cells. Plates were then  
579 inoculated at a MOI of 0.1 of SARS-CoV-2 in 50 µL of Opti-MEM for 1 hour at 37°C with  
580 occasional rocking. An additional 50 µL of fresh media was then added and incubated for 24  
581 hours at 37°C. Plates were fixed by submerging in 4% para-formaldehyde (PFA) in PBS for 1  
582 hour, then brought into BSL-1 for immunofluorescence staining. Permeabilization was  
583 performed with 2% bovine serum albumin (BSA), 0.1% Triton-X 100 in PBS for 1 hour at RT.  
584 Cells were stained with saRBD-1 at 2 µg/ml, mouse anti-dsRNA (Millipore sigma # MABE1134)  
585 1:1000. Anti-mouse IgG AF555 (Abcam ab150114) or anti-llama IgM AF488-conjugated  
586 secondary antibodies were added at 1:500 dilution for 1 hour at RT (Invitrogen). Confocal  
587 imaging was performed with a Zeiss LSM 980 using a 63x Plan-Achromatic 1.4 NA oil  
588 immersion objective. Images were processed with Zeiss Zen Blue software. Maximum intensity  
589 z-projections were prepared in ImageJ. All antibody stain images were pseudocolored for visual  
590 consistency.

591

### 592 **Flow cytometry of S transfected cells**

593 293T cells were seeded at 70% confluency on 24 well plates. Cells were then transfected with 1  
594 µg of HDM\_IDTSpike\_fixK S plasmid as described above. 24 hours after transfection, cells were  
595 harvested by scraping and immediately stained with live-dead 405nm stain Zombie Violet  
596 (BioLegend). After live-dead staining, cells were washed 2x with PBS, then fixed with 4% PFA  
597 for 15 minutes at RT. Cells were then washed 2x with PBS, then stained with saRBD-1 VHH at  
598 2 µg/ml, VHH52 at 2 µg/ml or phalloidin-Alexa Fluor 488 (AF488) (ThermoFisher Scientific  
599 A12379) for 1 hour at RT. Cells were washed 2x with PBS then treated with anti-VHH biotin

600 (Jackson 128-065-232) secondary antibody (Invitrogen #A16061) was added at 1:500 dilution  
601 for 1 hour at RT. Cells were then washed 2x with PBS and treated with streptavidin-AF488  
602 (Jackson 016-540-084) for 1 hour at RT. Cells were then resuspended in flow buffer (PBS, 3%  
603 FBS, 2mM EDTA), and filtered. Cells were then run on a BD FACSymphony flow cytometer with  
604 the assistance of the OHSU flow cytometry core.

605

### 606 **Thermal shift assay**

607 Purified RBD and saRBD-1 protein were diluted to 10  $\mu$ M in PBS. The combined RBD + saRBD-  
608 1 sample contained 10  $\mu$ M of each protein. SYPRO Orange dye was obtained as a 5000 $\times$   
609 solution (ThermoFisher) and was diluted to a final concentration of 5 $\times$  for all conditions.  
610 Experiments were performed on a StepOnePlus rtPCR system (Applied Biosystems) in a  
611 melting curve experiment with reporter set to ROX using a step and hold method starting at  
612 25°C, ramping at 1°C per minute until 95°C in a total reaction volume of 50  $\mu$ L per well. The  
613 melting point was calculated as the temperature with the minimum value of the first derivative of  
614 fluorescence emission as a function of temperature. The derivative values are calculated  
615 automatically by the StepOnePlus software and exported along with the normalized  
616 fluorescence intensity values.

617

### 618 **Spike-pseudotyped lentivirus production**

619 293T cells were seeded at 2 million cells/dish in 6cm TC-treated dishes. The following day, cells  
620 were transfected as described above with lentivirus packaging plasmids, SARS-CoV-2 S  
621 plasmid, and LzGreen as described above (Crawford et al., 2020). After transfection, cells were  
622 incubated at 37C for 48 hours. Viral media was harvested, filtered with 0.45 $\mu$ m filter, then frozen  
623 before use. Virus transduction capability was titered on 293T-ACE2 cells in DMEM plus 5  $\mu$ g/mL  
624 polybrene. LzGreen titers were determined by fluorescence using BZ-X700 all-in-one  
625 fluorescent microscope (Keyence): a 1:16 dilution was decided as optimal for following



626 neutralization assays due to broad transduced foci distribution. Each well was captured by  
627 Keyence microscope and stitched using built-in software. GFP signal was quantified for the  
628 stitched images using Keyence software, transduction levels were normalized to virus only  
629 control wells.

630

### 631 **Enzyme-linked immunosorbent assay (ELISA)**

632 MaxiSorp ELISA plates (Invitrogen), were coated with purified recombinant SARS-COV-2 RBD  
633 domain (BEI, NR-52306) at 2 µg/µl in PBS, or equivalent molar ratios of S1 domain (BEI, NR-  
634 53798), S2 domain (BEI, NR-53799), or trimer (BEI, NR-52396). Coating was carried out  
635 overnight at 4°C. Plates were blocked in wash buffer (2% BSA, 0.1% tween-20 in PBS) for 30  
636 minutes at RT. Dilutions ranging from 14.2 nM to 3 pM of saRBD-1 or Fc-saRBD-1 were  
637 incubated for 1 hour at RT. Plates were washed with PBST (0.1% tween-20 in PBS) 4 times  
638 between each antibody addition. Anti-VHH -biotinylated antibody and streptavidin -HRP  
639 secondary antibodies were used at 1:10000 concentration in blocking buffer and were incubated  
640 1 hour at RT. After the final wash, plates were incubated for 10 minutes with 50 µL of TMB HRP  
641 substrate (ThermoFisher) at RT, before adding 50 µL of stopping solution (2N H<sub>2</sub>SO<sub>4</sub>). Plate  
642 absorbances at 405nm were measured using a CLARIOstar® Plus plate fluorimeter (BMG  
643 Labtech).

644

### 645 **Biolayer interferometry (BLI)**

646 Streptavidin biosensors (ForteBio) were soaked in PBS for at least 30 minutes prior to starting  
647 experiments. Biosensors were prepared with the following steps: equilibration in kinetics buffer  
648 (10 mM HEPES, 150 mM NaCl, 3mM EDTA, 0.005% Tween-20, 0.1% BSA, pH 7.5) for 300  
649 seconds, loading of biotinylated RBD protein (10ug/mL) in kinetics buffer for 200 seconds, and  
650 blocking in 1 µM D-Biotin in kinetics buffer for 50 seconds. Binding was measured for seven 3-  
651 fold serial dilutions of each monoclonal antibody using the following cycle sequence: baseline

652 for 300 seconds in kinetics buffer, association for 300 seconds with antibody diluted in kinetics  
653 buffer, dissociation for 750 seconds in plain kinetics buffer, and regeneration by 3 cycles of 20  
654 seconds in 10 mM glycine pH 1.7, then 20 seconds in kinetics buffer. All antibodies were run  
655 against an isotype control antibody at the same concentration. For competition experiments,  
656 biosensors were loaded with RBD similarly to binding experiments, then bound with 50 nM  
657 saRBD-1 or 100 nM Fc-saRBD-1 for 300 seconds before transferring to monoclonal antibody  
658 diluted in kinetics buffer for 300 seconds (cov2rbdc2-mab10 was used at 20 nM, while srbdc4-  
659 mab10 and srbdc5-mab10 were used at 10 nM). Data analysis was performed using the  
660 ForteBio data analysis HT 10.0 software. Curves were reference subtracted using the isotype  
661 control and each cycle was aligned according to its baseline step.  $K_D$ 's were calculated using a  
662 1:1 binding model, and the kinetic parameters ( $K_D$ ,  $k_{ON}$ ,  $k_{OFF}$ ) were averaged from  
663 concentrations and replicates, excluding dilutions with an  $R_2$  less than 0.9 or an  $R_{max}$  more  
664 than double the average of other concentrations.

665

### 666 **Pseudovirus neutralization assay**

667 The neutralization protocol was based on previously reported neutralization methods utilizing  
668 SARS-CoV-2 S pseudotyped lentivirus (Crawford et al., 2020). 293T-ACE2 cells were seeded  
669 poly-lysine treated 96-well plates at a density of 10,000 cells per well. Cells were allowed to  
670 grow overnight at 37°C. LzGreen SARS-COV-2 S pseudotyped lentiviruses were mixed with  
671 saRBD-1, or VHH52 control antibody. Immunized alpaca serum was used as positive  
672 neutralization control, while virus alone was used as negative control. Dilutions of antibodies  
673 ranged from 177 nM to 170 pM for saRBD-1 and 26.3nM and 25 pM for Fc-saRBD-1, and 6.57  
674 nM to 4 pM Bi-saRBD-1. Virus-antibody mixture was incubated at 37C for 1 hour after which  
675 polybrene was added up to 5 µg/ml and the mixture was added to 293T-ACE2 cells. Cells were  
676 incubated with neutralized virus for 44 hours before imaging. Cells were fixed with 4% PFA for 1  
677 hour at RT. Fixed cells were washed with PBS 2x, then incubated with 10 µg/ml DAPI for 10

678 minutes at RT, imaged with BZ-X700 all-in-one fluorescent microscope (Keyence). Estimated  
679 area of DAPI and GFP fluorescent pixels were calculated with built in BZ-X software (Keyence).

680

### 681 **Focus forming assay (FFA)**

682 The FFAs was performed as previously described (Case et al., 2020). In brief, Vero E6 cells  
683 were plated at 20,000 cells/well or Caco-2 cells were plated at 24,000 cells/well in 96-well plates  
684 and incubated overnight. Titrated SARS-CoV-2 stocks were diluted to 3,333 ffu/mL. To 20  $\mu$ L of  
685 virus, 20  $\mu$ L of antibody dilutions were added: saRBD-1, VHH52, or Fc-saRBD-1 were used at  
686 8x4-fold serial dilutions ranging from 6.25  $\mu$ g/mL to 381 pg/mL for saRBD-1, 1.25  $\mu$ g/mL to 76.2  
687 pg/mL for Fc-saRBD-1, and 420  $\mu$ g/mL to 25.6 pg/mL All virus and antibody dilutions were  
688 prepared in Opti-MEM media. 30  $\mu$ L of neutralized virus was then added to the confluent cells  
689 and incubated for 1 hour at 37°C. 150  $\mu$ L of overlay media (Opti-MEM, 2% FBS, 2%  
690 Methylcellulose) was then added to each well and incubated for 24 hours at 37°C. Plates were  
691 fixed using 4% PFA for 1 hour at RT. Plates were then blocked for 30 minutes with  
692 permeabilization buffer (PBS, 0.1% BSA and 0.1% saponin). RBD immunized alpaca sera was  
693 used as a primary antibody at 1:5,000 dilution in permeabilization buffer, and anti-Llama-HRP  
694 secondary was used at 1:20,000 dilution in permeabilization buffer. Plates were developed in 30  
695  $\mu$ L TrueBlue (SeraCare) substrate and imaged with an Immunospot analyzer (CTL). Foci were  
696 counted with Viridot (Katzelnick et al., 2018) version 1.0 in R version 4.1.0.

697

### 698 **Quantification and statistical analysis**

699 For ELISA and neutralization data, EC<sub>50</sub> and IC<sub>50</sub> values were calculated using python software  
700 pipeline based on input data. Curves were fit to each data set using the same pipeline.  
701 For ELISA data, EC<sub>50</sub> were calculated from OD<sub>450</sub> nm signal relative to maximal signal for a  
702 given pattern. Background was subtracted, then each was normalized to the maximum value for  
703 that antigen. The S2 domain data was analyzed differently, as it was comparable to

704 background, background absorbance was first subtracted before normalization to maximum  
705 value.

706

707 For pseudovirus neutralization experiments, total surface area and intensity of blue and green  
708 signal were quantified using Keyence software. Three technical replicates were performed for  
709 each concentration in each experiment. The two values closest to the average of the triplicates  
710 were used to calculate the average of green signal (transduction), which was normalized to  
711 average blue signal (DAPI) for each concentration. The normalized transduction data were fit to  
712 a logistic function to determine  $EC_{50}$  and  $IC_{50}$  values in python version 3.8.10.

713

714 For live virus neutralization assays, focus counts generated with Viridot were manually checked  
715 for artifacts and recounted manually when incorrect. Focus counts were normalized in a plate-  
716 wise manner to the average of virus only well focus counts to obtain percent infection values,  
717 which were fit to a logistic function to determine  $FRNT_{50}$  values in python version 3.8.10.

718

### 719 **Acknowledgments**

720 BLI data were generated on an Octet Red 384, which is made available and supported by  
721 OHSU Proteomics Shared Resource facility and equipment grant number S10OD023413. We  
722 also thank the OHSU Flow Cytometry Shared Resource, and OHSU Advanced Light  
723 Microscopy Core for the use of their software, equipment, and expertise.

724

### 725 **Data availability**

726 The source data for this study are provided with the paper. SARS-CoV-2 RBD plasmid based on  
727 Wuhan isolate sequence from GenBank under accession number MN908947.3.

728

### 729 **Code availability**

730 No unique code was generated as part of this study.

731

732 **Author Contributions**

733 Conceptualization: F.G.T., J.B.W., and T.A.B.; methodology, formal analysis, and investigation:

734 T.A.B., J.B.W., H.C.L., and S.K.M.; writing – original draft: J.B.W., T.A.B.; writing – review and

735 editing: all authors; visualization: T.A.B., J.B.W., and F.G.T.; supervision: F.G.T.; project

736 administration: F.G.T.; fund acquisition: F.G.T.

737 **Lead contact**

738 Further information and requests for resources and reagents should be directed to the lead

739 contact, Fikadu G. Tafesse ([tafesse@ohsu.edu](mailto:tafesse@ohsu.edu))

740

741 **Declaration of interests**

742 The authors declare no competing interests

743

744

745

746

747

## 748 **References**

- 749 Amanat, F., Nguyen, T., Chromikova, V., Strohmeier, S., Stadlbauer, D., Javier, A., Jiang, K.,  
750 Asthagiri-Arunkumar, G., Polanco, J., Bermudez-Gonzalez, M., et al. (2020). A serological  
751 assay to detect SARS-CoV-2 seroconversion in humans (*Allergy and Immunology*).
- 752 Baden, L.R., El Sahly, H.M., Essink, B., Kotloff, K., Frey, S., Novak, R., Diemert, D., Spector,  
753 S.A., Roupheal, N., Creech, C.B., et al. (2021). Efficacy and Safety of the mRNA-1273 SARS-  
754 CoV-2 Vaccine. *New England Journal of Medicine* 384, 403–416.
- 755 Barnes, C.O., Jette, C.A., Abernathy, M.E., Dam, K.-M.A., Esswein, S.R., Gristick, H.B.,  
756 Malyutin, A.G., Sharaf, N.G., Huey-Tubman, K.E., Lee, Y.E., et al. (2020). SARS-CoV-2  
757 neutralizing antibody structures inform therapeutic strategies. *Nature* 588, 682–687.
- 758 Bates, T.A., Leier, H.C., Lyski, Z.L., McBride, S.K., Coulter, F.J., Weinstein, J.B., Goodman,  
759 J.R., Lu, Z., Siegel, S.A.R., Sullivan, P., et al. (2021a). Neutralization of SARS-CoV-2 variants  
760 by convalescent and BNT162b2 vaccinated serum. *Nat Commun* 12, 5135.
- 761 Bates, T.A., Leier, H.C., Lyski, Z.L., Goodman, J.R., Curlin, M.E., Messer, W.B., and Tafesse,  
762 F.G. (2021b). Age-Dependent Neutralization of SARS-CoV-2 and P.1 Variant by Vaccine  
763 Immune Serum Samples. *JAMA* 326, 868–869.
- 764 Bates, T.A., Weinstein, J.B., Farley, S., Leier, H.C., Messer, W.B., and Tafesse, F.G. (2021c).  
765 Cross-reactivity of SARS-CoV structural protein antibodies against SARS-CoV-2. *Cell Reports*  
766 34, 108737.
- 767 Bates, T.A., McBride, S.K., Winders, B., Schoen, D., Trautmann, L., Curlin, M.E., and Tafesse,  
768 F.G. (2022). Antibody Response and Variant Cross-Neutralization After SARS-CoV-2  
769 Breakthrough Infection. *JAMA* 327, 179–181.
- 770 Bierig, T., Collu, G., Blanc, A., Poghosyan, E., and Benoit, R.M. (2020). Design, Expression,  
771 Purification, and Characterization of a YFP-Tagged 2019-nCoV Spike Receptor-Binding Domain  
772 Construct. *Front. Bioeng. Biotechnol.* 0.
- 773 Carrillo, J., Izquierdo-Useros, N., Ávila-Nieto, C., Pradenas, E., Clotet, B., and Blanco, J. (2021).  
774 Humoral immune responses and neutralizing antibodies against SARS-CoV-2; implications in  
775 pathogenesis and protective immunity. *Biochem Biophys Res Commun* 538, 187–191.
- 776 Case, J.B., Rothlauf, P.W., Chen, R.E., Liu, Z., Zhao, H., Kim, A.S., Bloyet, L.-M., Zeng, Q.,  
777 Tahan, S., Droit, L., et al. (2020). Neutralizing Antibody and Soluble ACE2 Inhibition of a  
778 Replication-Competent VSV-SARS-CoV-2 and a Clinical Isolate of SARS-CoV-2. *Cell Host*  
779 *Microbe* 28, 475-485.e5.
- 780 Cavallari, M. (2017). Rapid and Direct VHH and Target Identification by Staphylococcal Surface  
781 Display Libraries. *Int J Mol Sci* 18.
- 782 Chen, R.E., Zhang, X., Case, J.B., Winkler, E.S., Liu, Y., VanBlargan, L.A., Liu, J., Errico, J.M.,  
783 Xie, X., Suryadevara, N., et al. (2021). Resistance of SARS-CoV-2 variants to neutralization by  
784 monoclonal and serum-derived polyclonal antibodies. *Nature Medicine* 1–10.

- 785 Crawford, K.H.D., Eguia, R., Dingens, A.S., Loes, A.N., Malone, K.D., Wolf, C.R., Chu, H.Y.,  
786 Tortorici, M.A., Veessler, D., Murphy, M., et al. (2020). Protocol and reagents for pseudotyping  
787 lentiviral particles with SARS-CoV-2 Spike protein for neutralization assays (Microbiology).
- 788 Crommelin, D.J.A., Anchordoquy, T.J., Volkin, D.B., Jiskoot, W., and Mastrobattista, E. (2021).  
789 Addressing the Cold Reality of mRNA Vaccine Stability. *Journal of Pharmaceutical Sciences*  
790 *110*, 997–1001.
- 791 Daniel, W., Nivet, M., Warner, J., and Podolsky, D.K. (2021). Early Evidence of the Effect of  
792 SARS-CoV-2 Vaccine at One Medical Center. *New England Journal of Medicine* *384*, 1962–  
793 1963.
- 794 Deng, X., Garcia-Knight, M.A., Khalid, M.M., Servellita, V., Wang, C., Morris, M.K., Sotomayor-  
795 González, A., Glasner, D.R., Reyes, K.R., Gliwa, A.S., et al. (2021). Transmission, infectivity,  
796 and neutralization of a spike L452R SARS-CoV-2 variant. *Cell* *184*, 3426-3437.e8.
- 797 Dong, E., Du, H., and Gardner, L. (2020). An interactive web-based dashboard to track COVID-  
798 19 in real time. *The Lancet Infectious Diseases* *20*, 533–534.
- 799 Eppendorf, N.S. Faster Isolation of PBMC Using Ficoll-Paque® Plus in the Eppendorf  
800 Multipurpose Benchtop Centrifuges 5920 R and 5910 Ri. 6.
- 801 Eroshenko, N., Gill, T., Keaveney, M.K., Church, G.M., Trevejo, J.M., and Rajaniemi, H. (2020).  
802 Implications of antibody-dependent enhancement of infection for SARS-CoV-2  
803 countermeasures. *Nat Biotechnol* *38*, 789–791.
- 804 Frei, J.C., and Lai, J.R. (2016). Protein and Antibody Engineering by Phage Display. *Methods*  
805 *Enzymol* *580*, 45–87.
- 806 Glasgow, A., Glasgow, J., Limonta, D., Solomon, P., Lui, I., Zhang, Y., Nix, M.A., Rettko, N.J.,  
807 Zha, S., Yamin, R., et al. (2020). Engineered ACE2 receptor traps potently neutralize SARS-  
808 CoV-2. *PNAS* *117*, 28046–28055.
- 809 Gordon, D.E., Jang, G.M., Bouhaddou, M., Xu, J., Obernier, K., O’Meara, M.J., Guo, J.Z.,  
810 Swaney, D.L., Tummino, T.A., Huttenhain, R., et al. (2020). A SARS-CoV-2-Human Protein-  
811 Protein Interaction Map Reveals Drug Targets and Potential Drug-Repurposing (Systems  
812 Biology).
- 813 Greaney, A.J., Starr, T.N., Gilchuk, P., Zost, S.J., Binshtein, E., Loes, A.N., Hilton, S.K.,  
814 Huddleston, J., Eguia, R., Crawford, K.H.D., et al. (2021). Complete Mapping of Mutations to the  
815 SARS-CoV-2 Spike Receptor-Binding Domain that Escape Antibody Recognition. *Cell Host &*  
816 *Microbe* *29*, 44-57.e9.
- 817 Günaydın, G., Yu, S., Gräslund, T., Hammarström, L., and Marcotte, H. (2016). Fusion of the  
818 mouse IgG1 Fc domain to the VHH fragment (ARP1) enhances protection in a mouse model of  
819 rotavirus. *Scientific Reports* *6*, 30171.
- 820 Güttler, T., Aksu, M., Dickmanns, A., Stegmann, K.M., Gregor, K., Rees, R., Taxer, W.,  
821 Rymarenko, O., Schünemann, J., Dienemann, C., et al. (2021). Neutralization of SARS-CoV-2  
822 by highly potent, hyperthermostable, and mutation-tolerant nanobodies. *EMBO J* *40*, e107985.

- 823 Hanke, L., Vidakovics Perez, L., Sheward, D.J., Das, H., Schulte, T., Moliner-Morro, A.,  
824 Corcoran, M., Achour, A., Karlsson Hedestam, G.B., Hällberg, B.M., et al. (2020). An alpaca  
825 nanobody neutralizes SARS-CoV-2 by blocking receptor interaction. *Nature Communications*  
826 *11*, 4420.
- 827 Hanke, L., Das, H., Sheward, D.J., Perez Vidakovics, L., Urgard, E., Moliner-Morro, A., Kim, C.,  
828 Karl, V., Pankow, A., Smith, N.L., et al. (2022). A bispecific monomeric nanobody induces spike  
829 trimer dimers and neutralizes SARS-CoV-2 in vivo. *Nat Commun* *13*, 155.
- 830 Hoffmann, M., Kleine-Weber, H., Schroeder, S., Krüger, N., Herrler, T., Erichsen, S.,  
831 Schiergens, T.S., Herrler, G., Wu, N.-H., Nitsche, A., et al. (2020). SARS-CoV-2 Cell Entry  
832 Depends on ACE2 and TMPRSS2 and Is Blocked by a Clinically Proven Protease Inhibitor. *Cell*  
833 *181*, 271-280.e8.
- 834 Hoffmann, M., Arora, P., Groß, R., Seidel, A., Hörnich, B.F., Hahn, A.S., Krüger, N., Graichen,  
835 L., Hofmann-Winkler, H., Kempf, A., et al. (2021). SARS-CoV-2 variants B.1.351 and P.1  
836 escape from neutralizing antibodies. *Cell* *184*, 2384-2393.e12.
- 837 Holder, J. Tracking Coronavirus Vaccinations Around the World. *The New York Times*.
- 838 Hu, X., Hu, C., Jiang, D., Zuo, Q., Li, Y., Wang, Y., and Chen, X. (2020). Effectiveness of  
839 Convalescent Plasma Therapy for COVID-19 Patients in Hunan, China. *Dose-Response* *18*,  
840 1559325820979921.
- 841 Huang, C., Wang, Y., Li, X., Ren, L., Zhao, J., Hu, Y., Zhang, L., Fan, G., Xu, J., Gu, X., et al.  
842 (2020). Clinical features of patients infected with 2019 novel coronavirus in Wuhan, China. *The*  
843 *Lancet* *395*, 497–506.
- 844 Ingram, J.R., Schmidt, F.I., and Ploegh, H.L. (2018). Exploiting Nanobodies' Singular Traits.  
845 *Annual Review of Immunology* *36*, 695–715.
- 846 Jiang, S., Hillyer, C., and Du, L. (2020). Neutralizing Antibodies against SARS-CoV-2 and Other  
847 Human Coronaviruses. *Trends Immunol* *41*, 355–359.
- 848 Jones, B.E., Brown-Augsburger, P.L., Corbett, K.S., Westendorf, K., Davies, J., Cujec, T.P.,  
849 Wiethoff, C.M., Blackbourne, J.L., Heinz, B.A., Foster, D., et al. (2021). The neutralizing  
850 antibody, LY-CoV555, protects against SARS-CoV-2 infection in nonhuman primates. *Science*  
851 *Translational Medicine*.
- 852 Kartoglu, U.H., Moore, K.L., and Lloyd, J.S. (2020). Logistical challenges for potential SARS-  
853 CoV-2 vaccine and a call to research institutions, developers and manufacturers. *Vaccine* *38*,  
854 5393–5395.
- 855 Katzelnick, L.C., Escoto, A.C., McElvany, B.D., Chávez, C., Salje, H., Luo, W., Rodriguez-  
856 Barraquer, I., Jarman, R., Durbin, A.P., Diehl, S.A., et al. (2018). Viridot: An automated virus  
857 plaque (immunofocus) counter for the measurement of serological neutralizing responses with  
858 application to dengue virus. *PLOS Neglected Tropical Diseases* *12*, e0006862.
- 859 Khoury, D.S., Cromer, D., Reynaldi, A., Schlub, T.E., Wheatley, A.K., Juno, J.A., Subbarao, K.,  
860 Kent, S.J., Triccas, J.A., and Davenport, M.P. (2021). Neutralizing antibody levels are highly  
861 predictive of immune protection from symptomatic SARS-CoV-2 infection. *Nat Med* 1–7.



- 862 Kim, C., Ryu, D.-K., Lee, J., Kim, Y.-I., Seo, J.-M., Kim, Y.-G., Jeong, J.-H., Kim, M., Kim, J.-I.,  
863 Kim, P., et al. (2021). A therapeutic neutralizing antibody targeting receptor binding domain of  
864 SARS-CoV-2 spike protein. *Nature Communications* 12, 288.
- 865 Koenig, P.-A., Das, H., Liu, H., Kümmerer, B.M., Gohr, F.N., Jenster, L.-M., Schiffelers, L.D.J.,  
866 Tesfamariam, Y.M., Uchima, M., Wuerth, J.D., et al. (2021). Structure-guided multivalent  
867 nanobodies block SARS-CoV-2 infection and suppress mutational escape. *Science*.
- 868 Korber, B., Fischer, W.M., Gnanakaran, S., Yoon, H., Theiler, J., Abfalterer, W., Hengartner, N.,  
869 Giorgi, E.E., Bhattacharya, T., Foley, B., et al. (2020). Tracking Changes in SARS-CoV-2 Spike:  
870 Evidence that D614G Increases Infectivity of the COVID-19 Virus. *Cell* 182, 812-827.e19.
- 871 Kumar, S., Chandele, A., and Sharma, A. (2021). Current status of therapeutic monoclonal  
872 antibodies against SARS-CoV-2. *PLOS Pathogens* 17, e1009885.
- 873 Laursen, N.S., Friesen, R.H.E., Zhu, X., Jongeneelen, M., Blokland, S., Vermond, J., Eijgen, A.  
874 van, Tang, C., Diepen, H. van, Obmolova, G., et al. (2018). Universal protection against  
875 influenza infection by a multidomain antibody to influenza hemagglutinin. *Science* 362, 598–  
876 602.
- 877 Levin, E.G., Lustig, Y., Cohen, C., Fluss, R., Indenbaum, V., Amit, S., Doolman, R., Asraf, K.,  
878 Mendelson, E., Ziv, A., et al. (2021). Waning Immune Humoral Response to BNT162b2 Covid-  
879 19 Vaccine over 6 Months. *New England Journal of Medicine* 0, null.
- 880 Liu, H., Zhang, Q., Wei, P., Chen, Z., Aviszus, K., Yang, J., Downing, W., Jiang, C., Liang, B.,  
881 Reynoso, L., et al. (2021a). The basis of a more contagious 501Y.V1 variant of SARS-CoV-2.  
882 *Cell Res* 31, 720–722.
- 883 Liu, J., Liu, Y., Xia, H., Zou, J., Weaver, S.C., Swanson, K.A., Cai, H., Cutler, M., Cooper, D.,  
884 Muik, A., et al. (2021b). BNT162b2-elicited neutralization of B.1.617 and other SARS-CoV-2  
885 variants. *Nature* 1–5.
- 886 Liu, L., Iketani, S., Guo, Y., Chan, J.F.-W., Wang, M., Liu, L., Luo, Y., Chu, H., Huang, Y., Nair,  
887 M.S., et al. (2021c). Striking Antibody Evasion Manifested by the Omicron Variant of SARS-  
888 CoV-2. *Nature* 1–8.
- 889 Luo, R., Delaunay-Moisan, A., Timmis, K., and Danchin, A. (2021). SARS-CoV-2 biology and  
890 variants: anticipation of viral evolution and what needs to be done. *Environmental Microbiology*  
891 23, 2339–2363.
- 892 Maass, D.R., Sepulveda, J., Pernthaner, A., and Shoemaker, C.B. (2007). Alpaca (*Lama pacos*)  
893 as a convenient source of recombinant camelid heavy chain antibodies (VHHs). *Journal of*  
894 *Immunological Methods* 324, 13–25.
- 895 Mast, F.D., Fridy, P.C., Ketaren, N.E., Wang, J., Jacobs, E.Y., Olivier, J.P., Sanyal, T., Molloy,  
896 K.R., Schmidt, F., Rutkowska, M., et al. (2021). Highly synergistic combinations of nanobodies  
897 that target SARS-CoV-2 and are resistant to escape. *ELife* 10, e73027.
- 898 Mathieu, E., Ritchie, H., Ortiz-Ospina, E., Roser, M., Hasell, J., Appel, C., Giattino, C., and  
899 Rodés-Guirao, L. (2021). A global database of COVID-19 vaccinations. *Nat Hum Behav* 1–7.

- 900 Pinto, D., Park, Y.-J., Beltramello, M., Walls, A.C., Tortorici, M.A., Bianchi, S., Jaconi, S., Culap,  
901 K., Zatta, F., De Marco, A., et al. (2020). Cross-neutralization of SARS-CoV-2 by a human  
902 monoclonal SARS-CoV antibody. *Nature* 583, 290–295.
- 903 Planas, D., Bruel, T., Grzelak, L., Guivel-Benhassine, F., Staropoli, I., Porrot, F., Planchais, C.,  
904 Buchrieser, J., Rajah, M.M., Bishop, E., et al. (2021). Sensitivity of infectious SARS-CoV-2  
905 B.1.1.7 and B.1.351 variants to neutralizing antibodies. *Nat Med* 27, 917–924.
- 906 Pymm, P., Adair, A., Chan, L.-J., Cooney, J.P., Mordant, F.L., Allison, C.C., Lopez, E., Haycroft,  
907 E.R., O'Neill, M.T., Tan, L.L., et al. (2021). Nanobody cocktails potently neutralize SARS-CoV-2  
908 D614G N501Y variant and protect mice. *Proc Natl Acad Sci U S A* 118.
- 909 Rotman, M., Welling, M.M., van den Boogaard, M.L., Moursel, L.G., van der Graaf, L.M., van  
910 Buchem, M.A., van der Maarel, S.M., and van der Weerd, L. (2015). Fusion of hlgG1-Fc to  
911 <sup>111</sup>In-anti-amyloid single domain antibody fragment VHH-pa2H prolongs blood residential time  
912 in APP/PS1 mice but does not increase brain uptake. *Nuclear Medicine and Biology* 42, 695–  
913 702.
- 914 Saerens, D., Kinne, J., Bosmans, E., Wernery, U., Muyldermans, S., and Conrath, K. (2004).  
915 Single Domain Antibodies Derived from Dromedary Lymph Node and Peripheral Blood  
916 Lymphocytes Sensing Conformational Variants of Prostate-specific Antigen. *J. Biol. Chem.* 279,  
917 51965–51972.
- 918 Salvador, J.-P., Vilaplana, L., and Marco, M.-P. (2019). Nanobody: outstanding features for  
919 diagnostic and therapeutic applications. *Anal Bioanal Chem* 411, 1703–1713.
- 920 Schmidt, F.I. (2018). Phenotypic Lentivirus Screens to Identify Antiviral Single Domain  
921 Antibodies. In *Influenza Virus: Methods and Protocols*, Y. Yamauchi, ed. (New York, NY:  
922 Springer New York), pp. 139–158.
- 923 Schoof, M., Faust, B., Saunders, R.A., Sangwan, S., Rezelj, V., Hoppe, N., Boone, M.,  
924 Billesbølle, C.B., Puchades, C., Azumaya, C.M., et al. (2020). An ultrapotent synthetic  
925 nanobody neutralizes SARS-CoV-2 by stabilizing inactive Spike. *Science* 370, 1473–1479.
- 926 Shan, D., Press, O.W., Tsu, T.T., Hayden, M.S., and Ledbetter, J.A. (1999). Characterization of  
927 scFv-Ig Constructs Generated from the Anti-CD20 mAb 1F5 Using Linker Peptides of Varying  
928 Lengths. *The Journal of Immunology* 162, 6589–6595.
- 929 Shen, X., Tang, H., Pajon, R., Smith, G., Glenn, G.M., Shi, W., Korber, B., and Montefiori, D.C.  
930 (2021). Neutralization of SARS-CoV-2 Variants B.1.429 and B.1.351. *New England Journal of*  
931 *Medicine* 0, null.
- 932 Shrotri, M., Navaratnam, A.M.D., Nguyen, V., Byrne, T., Geismar, C., Fragaszy, E., Beale, S.,  
933 Fong, W.L.E., Patel, P., Kovar, J., et al. (2021). Spike-antibody waning after second dose of  
934 BNT162b2 or ChAdOx1. *Lancet*.
- 935 Tiller, T., Meffre, E., Yurasov, S., Tsuiji, M., Nussenzweig, M.C., and Wardemann, H. (2008).  
936 Efficient generation of monoclonal antibodies from single human B cells by single cell RT-PCR  
937 and expression vector cloning. *Journal of Immunological Methods* 329, 112–124.

- 938 Wagner, T.R., Schnepf, D., Beer, J., Ruetalo, N., Klingel, K., Kaiser, P.D., Junker, D., Sauter,  
939 M., Traenkle, B., Frecot, D.I., et al. (2021). Biparatopic nanobodies protect mice from lethal  
940 challenge with SARS-CoV-2 variants of concern. *EMBO Rep* e53865.
- 941 Weinreich, D.M., Sivapalasingam, S., Norton, T., Ali, S., Gao, H., Bhore, R., Musser, B.J., Soo,  
942 Y., Rofail, D., Im, J., et al. (2021). REGN-COV2, a Neutralizing Antibody Cocktail, in Outpatients  
943 with Covid-19. *New England Journal of Medicine* 384, 238–251.
- 944 Wrapp, D., De Vlieger, D., Corbett, K.S., Torres, G.M., Wang, N., Van Breedam, W., Roose, K.,  
945 van Schie, L., Hoffmann, M., Pöhlmann, S., et al. (2020a). Structural Basis for Potent  
946 Neutralization of Betacoronaviruses by Single-Domain Camelid Antibodies. *Cell* 181, 1004-  
947 1015.e15.
- 948 Wrapp, D., Vlieger, D.D., Corbett, K.S., Torres, G.M., Breedam, W.V., Roose, K., Schie, L. van,  
949 Team, V.-C.C.-19 R., Hoffmann, M., Pöhlmann, S., et al. (2020b). Structural Basis for Potent  
950 Neutralization of Betacoronaviruses by Single-domain Camelid Antibodies. *BioRxiv*  
951 2020.03.26.010165.
- 952 Wu, Y., Wang, F., Shen, C., Peng, W., Li, D., Zhao, C., Li, Z., Li, S., Bi, Y., Yang, Y., et al.  
953 (2020). A noncompeting pair of human neutralizing antibodies block COVID-19 virus binding to  
954 its receptor ACE2. *Science* 368, 1274–1278.
- 955 Xiang, Y., Nambulli, S., Xiao, Z., Liu, H., Sang, Z., Duprex, W.P., Schneidman-Duhovny, D.,  
956 Zhang, C., and Shi, Y. (2020). Versatile and multivalent nanobodies efficiently neutralize SARS-  
957 CoV-2. *Science* 370, 1479–1484.
- 958 Xu, J., Xu, K., Jung, S., Conte, A., Lieberman, J., Muecksch, F., Lorenzi, J.C.C., Park, S.,  
959 Schmidt, F., Wang, Z., et al. (2021). Nanobodies from camelid mice and llamas neutralize  
960 SARS-CoV-2 variants. *Nature*.
- 961 Yuan, M., Wu, N.C., Zhu, X., Lee, C.-C.D., So, R.T.Y., Lv, H., Mok, C.K.P., and Wilson, I.A.  
962 (2020). A highly conserved cryptic epitope in the receptor binding domains of SARS-CoV-2 and  
963 SARS-CoV. *Science* 368, 630–633.
- 964 Zeng, H., Wang, D., Nie, J., Liang, H., Gu, J., Zhao, A., Xu, L., Lang, C., Cui, X., Guo, X., et al.  
965 (2020). The efficacy assessment of convalescent plasma therapy for COVID-19 patients: a  
966 multi-center case series. *Sig Transduct Target Ther* 5, 1–12.
- 967 Zhang, X., Wu, S., Wu, B., Yang, Q., Chen, A., Li, Y., Zhang, Y., Pan, T., Zhang, H., and He, X.  
968 (2021). SARS-CoV-2 Omicron strain exhibits potent capabilities for immune evasion and viral  
969 entrance. *Sig Transduct Target Ther* 6, 1–3.
- 970 Zupancic, J.M., Schardt, J.S., Desai, A.A., Makowski, E.K., Smith, M.D., Pornnoppadol, G.,  
971 Garcia de Mattos Barbosa, M., Cascalho, M., Lanigan, T.M., and Tessier, P.M. (2021).  
972 Engineered Multivalent Nanobodies Potently and Broadly Neutralize SARS-CoV-2 Variants.  
973 *Advanced Therapeutics* 4, 2100099.
- 974